Spatial and temporal variations of the seasonal sea level cycle in the northwest Pacific

Article

Accepted Version

Feng, X. ORCID: https://orcid.org/0000-0003-4143-107X, Tsimplis, M. N., Marcos, M., Calalfat, F. M., Zheng, J., Jorda, G. and Cipollini, P. (2015) Spatial and temporal variations of the seasonal sea level cycle in the northwest Pacific. Journal of Geophysical Research: Oceans, 120 (10). pp. 7091-7112. ISSN 2169-9291 doi: 10.1002/2015JC011154 Available at https://centaur.reading.ac.uk/44451/

www.reading.ac.uk/centaur

1

Spatial and temporal variations of the seasonal sea level cycle in

the northwest Pacific

4

5   Xiangbo Feng[1,2,3*], Michael N. Tsimplis[2], Marta Marcos[4], Francisco M. Calafat[2],

6   Jinhai Zheng[3], Gabriel Jordà [4] and Paolo Cipollini[2]

7

8   1. Department of Meteorology, University of Reading, Reading, UK

9   2. National Oceanography Centre, Southampton, UK

10   3. Hohai University, Nanjing, China

11   4. IMEDEA (CSIC–UIB), Esporles, Spain

12

13   * Corresponding author: Xiangbo Feng (xiangbo.feng@reading.ac.uk)

14

15

16   **Abstract**

17   The seasonal sea level variations observed from tide gauges over 1900-2013 and

18   gridded satellite altimeter product AVISO over 1993-2013 in the northwest

19   Pacific have been explored. The seasonal cycle is able to explain 60-90% of

20   monthly sea level variance in the marginal seas, while it explains less than 20%

21   of variance in the eddy-rich regions. The maximum annual and semi-annual sea

22   level cycles (30cm and 6cm) are observed in the north of the East China Sea and

23   the west of the South China Sea respectively. AVISO was found to underestimate

24   the annual amplitude by 25% compared to tide gauge estimates along the coasts

25   of China and Russia.

26   The forcing for the seasonal sea level cycle was identified. The atmospheric

27   pressure and the steric height produce 8-12cm of the annual cycle in the middle

28   continental shelf and in the Kuroshio Current regions separately. The removal of

29   the two attributors from total sea level permits to identify the sea level residuals

30   that still show significant seasonality in the marginal seas. Both nearby wind

31   stress and surface currents can explain well the long-term variability of the

32   seasonal sea level cycle in the marginal seas and the tropics because of their

33   influence on the sea level residuals. Interestingly, the surface currents are a

34   better descriptor in the areas where the ocean currents are known to be strong.

35   Here, they explain 50-90% of inter-annual variability due to the strong links

36   between the steric height and the large-scale ocean currents.

37

1. Introduction

The seasonal cycle, and more specifically its annual and semi-annual components, dominates the non-tidal variability of sea level in many regions of the ocean. Because the seasonal variability is very energetic for monthly sea level records and also it is auto-correlated, this signal is normally removed from the estimation of trends of mean sea level. However, this does not hide the practical significance of the seasonal cycle. Coastal infrastructure is more vulnerable at the time when the seasonal sea level cycle is at its highest [*Tsimplis and Shaw,* 2010; *Dangendorf et al.,* 2013a*; Torres and Tsimplis*, 2014], and the decadal increases in the seasonal cycle will make the vulnerability of the coastal areas even higher. The seasonal changes in stratification, which are seen in the seasonal sea level cycle, can cause significant seasonal changes in tides [*Kang et al*., 2002; *Müller et al*., 2014], leading to the prediction of tides and extremes more complicated. Furthermore, the seasonal sea level cycle is firmly regulating the seawater-freshwater balance both under the ground [*Michael, et al*., 2005] and at the river estuaries [*Anderson and Lockaby*, 2012], and it acts as a key factor determining the seawater intrusion. Therefore, obtaining good physical understanding of the processes involved in determining the seasonal sea level cycle and its spatial and temporal changes enables us to assess the extent of future changes in climate that will impact on the coastal ocean environments.

The gravitational forcing contributes very little (in mm) to the observed seasonal sea level cycle [*Pugh and Woodworth*, 2014]. Seasonality in meteorological, oceanographic and hydrological processes is considered to force the seasonal sea level cycle, but the contribution of each factor varies spatially and temporally

62   [*Plag and Tsimplis*, 1999; *Marcos and Tsimplis*, 2007; *Hünicke and Zorita*, 2008;

63   *Vinogradov et al.*, 2008; *Torres and Tsimplis*, 2012; *Dangendorf et al.,* 2013b;

64   *Wahl et al.,* 2014]. Notably, temporal changes in the seasonal sea level cycle may

65   be caused by the sea level components which are not the dominant ones.

66   Therefore, mapping the seasonal sea level cycle, identifying the dominant

67   components regionally and furthermore identifying the forcing of its temporal

68   changes is very important in order to understand the physics of the sea level

69   variability at the seasonal frequencies.

70   On the basis of tide gauge data, *Tsimplis and Woodworth* [1994] mapped the

71   features of the seasonal sea level cycle in coastal waters, showing spatial

72   variability but also regional coherence. Satellite radar altimetry has the

73   capability of monitoring the sea level variations with a better spatial coverage,

74   and the native altimetric along-track data are often gridded for further use of

75   analysis and visualization. *Chen et al.* [2000] explored the estimations of the

76   seasonal cycle in open oceans using gridded altimeter measurements. However,

77   at the continental coasts the altimetry was found to significantly underestimate

78   the annual level cycle [*Han and Huang,* 2008; *Vinogradov and Ponte,* 2010]. This

79   underestimation is normally caused by a combination of data flagging (in turn

80   due to contamination of the altimetric waveforms and/or inadequacy of some of

81   the corrections such as the one compensating for path delay due to water vapour)

82   and data filtering in the last 20-30 km from the coasts. For the gridded altimeter

83   data, the mapping procedure additionally tends to smooth the characteristics of

84   the local phenomena of sea level that are captured by the tide gauges. For each

85   region, it is vital to clearly identify the uncertainty of the altimeter products in

86   estimating the seasonal sea level before using their results into other fields. It is

87   worth noting that considerable research efforts are being put into improving the

88   along-track altimetry in the coastal zone [*Vignudelli et al.*, 2011]. The latest

89   coastal altimetry products reprocessed with improved techniques allow a better

90   representation of sea level variability near the coasts [*Passaro et al.*, 2015] but

91   those products are not yet available for all the past missions and coastal areas

92   and therefore time series are limited.

93   The stability of the seasonal sea level cycle with time has also been studied for a

94   few regions where long-term tide gauge records exist. The annual cycle

95   amplitude was found to exhibit decadal variations between 1 to 20 cm in the

96   European coasts [*Plag and Tsimplis*, 1999; *Barbosa et al.,* 2008; *Hünicke and*

97   *Zorita*, 2008*; Dangendorf et al.,* 2013b], the Mediterranean Sea [*Marcos and*

98   *Tsimplis*, 2007], the Caribbean Sea [*Torres and Tsimplis*, 2012] and the South

99   China Sea [*Amiruddin et al.*, 2015]. Interestingly, the annual cycle amplitude

100   along the US Gulf coast was recently reported to have increased by 20-30% since

101   1990s, and the sea surface air temperature was argued as an indicator for the

102   increase [*Wahl et al.,* 2014]. These studies are all based on the traditional annual

103   cycle definitions, assuming that both amplitude and frequency of the annual

104   cycle are constant within each time segment of assessments but that they are

105   allowed to change over different segments. Consequently, there is a possibility

106   that the inter-annual or even lower-frequency variability in the monthly values

107   may be treated as part of the annual cycle signal if the length of assessment

108   windows is not appropriate. An alternative method, the modulated annual cycle

109   that allows the annual cycle parameters to change instantaneously, was

110   introduced to the climate analysis by *Wu et al.* [2008]. Based on this concept,

111   some reconstruction products have been made to recover the high- and low-

112   frequency signals in sea level [*Hamlington et al.*, 2010, 2011 and 2012].

113   The northwest Pacific is a region where both oceanographic and atmospheric

114   dynamics (e.g. the western boundary currents, the monsoon and typhoons) are

115   known to have strong impacts on the sea surface processes. The areas studied

116   here are of particular interest also because they are heavily populated areas

117   where intensive anthropogenic activities were found to have significantly

118   changed the coastal geomorphology [*Wang et al.,* 2014, and references therein].

119   *Marcos et al.* [2012] identified the spatial and temporal variations of mean sea

120   level in the marginal seas of this region and associated them with the large-scale

121   climatic variability. *Feng et al*. [2015] explored the long-term changes in tidal

122   signals and proposed them as the consequences of the anthropogenic activities.

123   These sea level components were suggested to consequently alter the

124   occurrence of extremes [*Feng and Tsimplis,* 2014]. However, the seasonal cycle,

125   as a crucial component in sea level, has not been systematically studied over the

126   whole region of the northwest Pacific. The dynamics behind the spatial and

127   temporal variations remain unrevealed.

128   This paper provides a regional investigation on the seasonal sea level cycle over

129   the northwest Pacific, by using publically accessible datasets, which include tide

130   gauge records, gridded satellite altimetry data and atmospheric and oceanic

131   reanalysis. Four questions are addressed. Firstly, what are the spatial features of

132   the seasonal sea level cycle in this region; secondly, to what extent can gridded

133   satellite altimetry product estimate the coastal seasonal sea level cycle; thirdly,

134 how much do the seasonal signals change with time; and fourthly, what are the

135 causes for the seasonal sea level oscillations and for their long-term variability as

136 well, and to what extent can each of the contributors explain the variability.

137 The paper is structured as follows. In section 2, the data processing of sea level

138 observations and atmospheric and oceanic climate reanalysis used are described

139 together with the methodologies. In Section 3, spatial features of the seasonal sea

140 level cycle are investigated, and harmonic parameters estimated from tide

141 gauges and gridded altimetry data are compared. Temporal variability of the

142 seasonal cycle is also addressed in this section. In Section 4, mechanisms for the

143 spatial and temporal changes of the seasonal sea level cycle are explored,

144 including the atmosphere pressure loading, the ocean thermal

145 expansion/contraction and freshwater content, the wind stress and the sea

146 surface currents. Finally, the conclusions are given in Section 5.

147

148 **2. Data and methodology**

149 **2.1 Sea level observational records**

150 Monthly sea level data (η) recorded at 120 tide gauges in the northwest Pacific

151 were obtained from the Permanent Service for Mean Sea Level [*Holgate et al.*,

152 2013]. Locations and numbering of the 120 tide gauge stations are provided in

153 **Figure 1a**. Tide gauges are classified into 6 sub-regions: the east of the South

154 China Sea (SCS-E) (station number: 1-14), the west of the South China Sea (SCS-

155 W) (station number: 15-39), the East China Sea (ECS) (station number: 40-61),

156   the Sea of Japan (SoJ) (station number: 62-89), the northeast coasts of Japan

157   (Japan-NE) (station number: 90-105) and the southeast coasts of Japan (Japan-

158   SE) (station number: 106-115). There are two stations on the coasts of the Sea of

159   Okhotsk (station number: 119 and 120) and three stations in the south of Japan

160   (station number: 116-118) where the observed seasonal sea level cycle has

161   different behaviour from that at neighboring sites (this will be discussed in

162   subsection 3.3). Thus, these five stations are taken as outliers relative to above 6

163   sub-regions. The dataset used spans the period 1900-2013. However, only a few

164   stations have records longer than 50 years (**Figure 1b**). The minimum record

165   length used in the analysis was 16 years. The dataset contains 105 revised local

166   reference records and 15 metric records. The metric records do not contain the

167   information about the benchmark datum contributed by re-leveling adjustments

168   to a certain level, but they can be useful for studies of the seasonal sea level cycle

169   if they are carefully treated.

170   The data quality control of tide gauge records performed included the visual

171   checks of time series and the adjustment or removal of values over periods with

172   spurious shifts. Although it is not necessary to know the actual level of the datum

173   for estimating the seasonal cycle, the stability of the datum is still important for

174   assessing the temporal variability of the cycle. Where a record showed datum

175   shifts over different segments these were adjusted to the same reference level by

176   removing their mean values after each segment was detrended. Sea level values

177   that showed obvious jumps or shifts after the known earthquakes were also

178   excluded. Two massive earthquakes were considered, which stroke the Kuril

179   Islands on the 4th October 1994 and the Oshika Peninsula on the 11th March 2011

8

180   respectively (www.nodc.noaa.gov/outreach/esm). For individual records, mean

181   values and trends were removed and then plotted into 6 groups as specified

182   above. In each group, if parts of records show spurious jumps or shifts compared

183   with other members, or go beyond the spreading edges of the ensembles, these

184   records are omitted. **Figure 1b** gives the period of valid data at each station after

185   the quality control.

186   Gridded satellite radar altimeter data that cover the northwest Pacific (0-65°N,

187   100°E -170°E) were also used. The data were produced by SSALTO/DUACS and

188   distributed by AVISO, with support from CNES

189   (http://www.aviso.altimetry.fr/duacs/). The data consist of monthly averaged

190   maps of sea level anomalies, corresponding to multimission gridded sea surface

191   height anomaly (including Saral, Cryosat-2, Jason-1&2, T/P, Envisat, GFO, ERS-

192   1&2 and Geosat) with respect to a 21-year mean sea level. The spatial resolution

193   of the gridded altimeter data is 1/4° × 1/4 °, which permits resolving the sea

194   level related to the mesoscale eddies. Oceanic and atmospheric dynamics are

195   routinely corrected in the mission track data. These include the ocean tide, the

196   pole tide and the dynamic atmospheric correction (DAC) [*Carrère and Lyard*,

197   2003]. Because the inverted barometer (IB) effect (η_{IB}) has been corrected in the

198   AVISO data, we here refer to the monthly sea level records from AVISO as $\eta - \eta_{IB}$.

199   **2.2 Atmospheric pressure data and the IB effect**

200   In the open ocean, the sea level is assumed to isostatically react to the

201   atmospheric pressure loading on the sea surface by the inverted barometer (IB)

202   effect (η_{IB}) [*Gill*, 1982; *Wunsch and Stammer*, 1997; *Ponte*, 2006]. η_{IB} =-1/ρg(P-

203   P_{ref}), where ρ and g are the water density and gravity acceleration respectively,

204   and P-P_{ref} is the fluctuation of sea level pressure P relative to a long-term

205   average P_{ref} over the global ocean [*Wunsch and Stammer*, 1997; *Ponte*, 2006].

206   The consequence of a 1-mbar increase in surface pressure is approximately 1cm

207   depression of sea level.

208   With respect to the tide gauge records, the monthly sea level pressure data over

209   1900-2013 were used to calculate η_{IB} closest to the stations. The pressure data

210   were obtained by combining the NOAA's 20th century reanalysis v2 for the

211   period 1900-2012 [*Compo et al.*, 2011] and the ECMWF-Interim for 2013. Please

212   note that for each tide gauge record η_{IB} is only applied over the periods when

213   the tide gauge has valid data.

214   For AVISO records, the monthly average of 6-hour dynamic atmospheric

215   corrections (DAC) was used as η_{IB} over the sea surface. The DAC data are the sea

216   level variability combining the high-frequency signals (less than 20 days) due to

217   atmospheric wind and pressure forcing and low-frequency signals (more than 20

218   days) from the static IB correction on the atmospheric pressure. The monthly

219   average of DAC is equivalent to the isostatic IB effect [*Pascual et al.*, 2008]. The

220   DAC data are produced by CLS Space Oceanography Division using the Mog2D

221   model from Legos [*Carrère and Lyard*, 2003] and distributed by AVISO.

222   **2.3 Ocean temperature and salinity analysis and the steric height**

223   The steric height was calculated from the 3D hydrographic gridded product

224   EN4.0.2 generated by the UK Met Office Hadley Centre. This product has been

225   generated through the objective analysis of a global quality controlled dataset of

226   ocean temperature and salinity profiles, and is provided on a grid with 1° spatial

227   resolution in the horizontal and 42 levels in the vertical [*Good et al.*, 2013]

228   covering the period 1900-2013. The main observational data source is WOD09

229   [*Boyer et al.,* 2009]. The steric component of seasonal sea level change is mainly

230   due to the water density changes over the thermocline depth [*Chen et al.*, 2000;

231   *Vinogradov et al.,* 2008; *Torres and Tsimplis*, 2012]. Therefore, the values over

232   the top 500m were used in the calculation of the steric signal.

233   The steric height (η_{ster}), consisting of thermosteric (η_{thermo}) and halosteric

234   components (η_{halo}), over water depth (*H)* can be expressed as:

$$\eta_{thermo} = \int_{-H}^{0} C \cdot \Delta T\, dz$$

(1)

$$\eta_{halo} = \int_{-H}^{0} D \cdot \Delta S\, dz$$

235   where ΔT and ΔS are the temperature and salinity fluctuation relative to the

236   mean values over the whole period of study at each layer, and C and D are the

237   thermal expansion and salt compression coefficients respectively [*Tabata*, 1986].

238   C and D are defined as

$$C = -\frac{1}{\rho}\frac{\partial \rho}{\partial T}$$

(2)

$$D = -\frac{1}{\rho}\frac{\partial \rho}{\partial S}$$

11

239   where ρ is the water density, depending on water depth, temperature and

240   salinity, and is defined by the Joint Panel on Oceanographic Tables and Standards

241   [*UNESCO*, 1981].

242   η_{ster} calculated at tide gauge stations or shallow water regions is usually very

243   small and cannot represent the entire seasonal steric signal. Thus we used the

244   values at deep grid points (over 500m) closest to the sites of interest. This

245   method assumes that the whole steric signal in the deep ocean is transmitted to

246   the coast [*Bingham and Hughes*, 2012].

247   We also repeated the above process to calculate η_{ster} based in the 3D gridded

248   oceanic properties from the Simple Ocean Data Assimilation (SODA), which will

249   be introduced later, in order to explain the mechanisms of the long-term

250   variations of the seasonal sea level cycle.

251   **2.4 Ocean reanalysis SODA**

252   The sea surface height without the IB effect ($\eta - \eta_{IB}$), 3D ocean temperature and

253   salinity, the wind stress and the sea surface currents from the Simple Ocean Data

254   Assimilation (SODA) v2.2.4 covering the period 1900-2010 were also used to

255   understand the forcing of the seasonal sea level cycle. The SODA reanalysis is

256   based on the Parallel Ocean Program ocean model [*Smith et al.,* 1992], with 0.25°

257   × 0.4° horizontal resolution and 40 vertical levels, and assimilates oceanic data

258   through an optimal interpolation method every 10 days [*Carton et al.*, 2000]. In

259   the version v2.2.4 [*Giese and Ray*, 2011], the observations used in the data

260   assimilation scheme only include the ocean temperature and salinity profiles

261   from WOD09 [*Boyer et al.,* 2009] (it is also the main data source for the Met

262   Office Hadley Centre EN4) and sea surface temperature from ICOADS 2.5

263   [*Woodruff et al.,* 2011]. Thus, SODA is expected to be able to seasonally

264   represent the steric height in sea level. It is worth noting that SODA does not

265   assimilate sea level observations (i.e. from altimetry or tide gauges). The model

266   is forced with atmospheric fields from the NOAA's 20th century reanalysis v2

267   [*Compo et al.,* 2011] over the period 1871-2010 [*Carton and Giese*, 2008]

268   We use SODA for the purpose of identifying the forcing of the seasonal sea level

269   cycle (the method used in estimating the seasonal sea level cycle will be

270   described in the next subsection). To do so it is necessary to first assess the

271   capability of SODA in describing the observed seasonal sea level cycle in this

272   region. Please note that because SODA does not include the IB effect, in the

273   assessment η_{IB} was excluded both in AVISO data and in tide gauge records,

274   ensuring that the three datasets are all free of the IB effect. Details of the

275   assessment are provided in the supplementary materials. The comparison

276   results are summarized as: 1) the mean seasonal sea level cycle determined by

277   SODA over 1993-2010 is in good agreement with the estimations observed by

278   AVISO over 1993-2013 in most areas, with some discrepancies for annual

279   amplitudes below 3-6 cm and mainly occurring at the coastal regions (**Figure

280   S1-S2**); 2) the inter-annual variability of the seasonal sea level cycle over 1900-

281   2010 from SODA has significant correlation with the results observed at most of

282   the tide gauge records (in 96 of 120), with *R*=0.59 and 0.58 on average for annual

283   and semi-annual amplitudes respectively, and the worse representation of SODA

284   is mainly in the north of East China Sea and the north of the Sea of Japan where

285   the tide gauge records are relatively short (**Figure S3**); and 3) when the regional

286   average is concerned, SODA can well represent the inter-annual variability of the

287   seasonal sea level cycle for each sub-region (**FigureS4**), with correlation R=0.61

288   and 0.57 on average for annual and semi-annual amplitudes against tide gauge

289   observations. Thus, we conclude that SODA reproduces the seasonal sea level

290   cycle in the area of study with a reasonable accuracy and we will use it in the

291   characterization of the forcing mechanisms that determine the seasonal cycle.

292   It should be kept in mind that discrepancies of SODA still exist in the seasonal

293   sea level cycle estimations. This can be due to many different aspects of SODA,

294   such as the quality of atmospheric forcing, the low resolutions of the model at

295   coasts, the non-conserving global water mass [*Tamisiea et al.*, 2010], or the non-

296   conserving budgets in the ocean data assimilation procedure [*Haines et al.*,

297   2012]. More efforts are needed to interpret the skills of SODA, but this is not the

298   scope of this paper.

299   **2.5 Regression model for seasonal cycle**

300   The harmonic parameters of the annual and semi-annual cycles were estimated

301   through least squares fitting to the monthly records by the following equation:

$$\eta(t) = \beta_0 + A_a \cos\left(\frac{2\pi}{12}(t - \phi_a)\right) + A_{sa} \cos\left(\frac{2\pi}{6}(t - \phi_{sa})\right) \quad (3)$$

302   where $\eta(t)$ is the monthly mean value of sea level at time t (in units of months

303   and corresponding to the middle of January), β_0 is the estimated mean value, and

304   A_a and A_{sa} are the annual and semi-annual amplitudes corresponding to the

305   phase lags of ϕ_a and ϕ_{sa} respectively. The significance of the estimated harmonic

14

306   parameters was tested at 95% confidence level by assuming the regression

307   errors are normally distributed. Note that all the monthly records used in the

308   analysis were detrended over the period before being fitted by Eq.(3).

309   The mean seasonal cycle for each sea level record was estimated on the basis of

310   Eq. (3) using the data over the whole period. The temporal variability of the

311   seasonal cycle was also estimated on the basis of applying Eq. (3) for 5-year

312   segments shifted year-by-year. The 5-year length of data segment was chosen as

313   suggested by *Tsimplis and Woodworth* [1994] as a period over which most

314   records provide stable estimates for the seasonal cycle.

315   We applied this method to different sea level components, the wind stress and

316   the sea surface currents, to diagnose the forcing mechanisms of the seasonal sea

317   level cycle. In estimating the temporal variability of the seasonal cycle for the

318   wind stress and the sea surface currents, the two variables as 2D vectors are

319   equally divided into 18 sections (0-180° relative to the east anticlockwise by

320   10°) to get their values at different directions. This process permits us to

321   distinguish the vectors with the direction that have the best correlations with the

322   seasonal sea level variations.

323

324   **3. Seasonal sea level cycle from observations**

325   **3.1 Monthly sea level variations**

326   The monthly variances of η from tide gauges and AVISO are shown in **Figure 2a**.

327   Note that η from AVISO is obtained by adding η_{IB} (DAC data) back to $\eta - \eta_{IB}$

328   (AVISO sea level records). The variance exceeds 300 cm^2 in the north of the East

329   China Sea and in regions with strong western boundary currents, i.e. the

330   Kuroshio Extension and the south Oyashio Currents. Values of 150-200 cm^2 are

331   found in the East China Sea, the Luzon Strait, the Gulf of Thailand and the area of

332   the Equatorial Current.

333   **Figure 2b** shows the percentage of variance explained by the seasonal cycle

334   regression model of Eq.(3). The regression model explains 60-90% of the

335   variance in the vast majority of areas of the marginal seas over the continental

336   shelf, except in the Sea of Okhotsk where sea ice usually exists in cold seasons

337   [*Parkinson et al.,* 1999]. In the open ocean the percentage of variance explained

338   by the seasonal cycle is very low, except in a zonal band (10°N -20°N) and in the

339   west of the ocean interior where 40-50% of sea level variance can be attributed

340   to the seasonal cycle. It is worth noting that in the regions of the Kuroshio

341   Extension and the south Oyashio Currents, where the sea level variance is

342   maximum (**Figure 2a**), the seasonal cycle captures less than 20% of variance

343   (**Figure 2b**). The low representativeness of the seasonal cycle in the open ocean

344   can be interpreted by the presence of eddies which have the strong signature in

345   sea level (and thus induce high variance in sea level observations) but which

346   usually have much irregular seasonal variations. In fact, this region has been

347   identified as the region with the richest mesoscale eddies in the world [*Chelton et*

348   *al.,* 2011].

349   The sea level variance observed by AVISO at the closest points to tide gauges is

350   lower than that observed by tide gauges at 96 of the 120 stations. The difference

351   of variance (AVISO – tide gauges) is -31 cm^2 on average (21% of variance

352   determined by tide gauges). The largest discrepancies occur in the north of the

353   Philippines and at the west of the South China Sea (**Figure 2a**). When the period

354   of AVISO (1993-2013) is considered, there are 103 tide gauge records having

355   valid data over the period. AVISO is then found to underestimate the sea level

356   variance again at 64 of the 103 stations by overall -16 cm^2 (11% of variance by

357   tide gauges). Thus, we conclude that AVISO underestimates the coastal sea level

358   variance at most of stations disregarding the period.

359   In the estimations, the annual and semi-annual cycle parameters in Eq.(3) are

360   assumed to be constant during the whole period of records. Actually, as we will

361   discuss later, they could change in time. Thus, we cannot rule out the possibility

362   that the sea level variance accounted by the seasonal cycle and the resulting

363   percentages as indicated above may change when different periods of time are

364   considered.

365   **3.2 Mean seasonal sea level cycle**

366   The annual cycle of η is significant at all tide gauge records and in most areas

367   (**Figure 3a-b**). The values of A_a exceed 15cm in the East China Sea, the south of

368   Japan, the areas of the Kuroshio Current, the Luzon Strait and the Gulf of

369   Thailand. A_a is less than 3cm or becomes statistically insignificant in the equator

370   area (0-10°N) and the Sea of Okhotsk. The highest A_a (29±1cm) occurs at the

371   north of the East China Sea (station number: 47 and 48). The annual phase ϕ_a is

372   in December-January in the equator area, while it changes to August-November

373   when heading to north. ϕ_a is not uniform in each basin, except in the East China

374   Sea.

17

375   The semi-annual cycle is significant at most of tide gauge records (113 of 120), in

376   the equator area and in most areas of marginal seas, except in the Sea of Japan

377   (**Figure 3c-d**). A_{sa} has the highest values of 5-7cm in the northwest of the South

378   China Sea and in the Kuroshio Extension area. ϕ_{sa} is changing from January to

379   May (or July to November) when heading to south, and the direction of ϕ_{sa}

380   change is in opposite to that of ϕ_a change (**Figure 3b**).

381   The comparisons of the annual and semi-annual parameters derived from AVISO

382   and tide gauge measurements are shown in **Figure 4**. The differences are

383   regarded as significant if the error bars of the two compared values do not

384   overlap. At the points closest to tide gauges, AVISO significantly underestimates

385   A_a at 59 of the 120 stations by 2-9cm, with 3.5cm on average (25% of tide

386   gauges estimates), and overestimates at 2 stations (station number: 6 and 93) by

387   1.4cm and 2.2cm (37% and 42% of tide gauge estimates) (**Figure 4a**). Large

388   underestimations of 5-8cm ($\sim$40% of tide gauges values) are found in the west of

389   the South China Sea, the East China Sea and the Sea of Japan. Meanwhile, ϕ_a

390   derived from AVISO is significantly advanced by 10-35 days at 18 stations and

391   delayed by 5-12 days at 4 stations (**Figure 4b**). The semi-annual cycle is

392   detectable at 113 stations for tide gauge measurements but only detectable at

393   the corresponding AVISO points for 87 stations. AVISO underestimates A_{sa} by 1-

394   3cm (60%) at 28 of the 87 stations, while discrepancies of ϕ_{sa} occur at only 8

395   stations when the error bars are considered (**Figure 4c-d**).

396   The discrepancies of the seasonal sea level cycle estimated from AVISO still

397   remain when the common period (1993-2013) is used at tide gauge records for

398   the comparisons. We also found that the differences of harmonic parameters

18

399   derived from AVISO and tide gauges can well explain the discrepancies of the sea

400   level variance in most of the coastal areas, which have been identified in

401   subsection 3.1. This indicates that the underestimation of the seasonal cycle

402   amplitudes is consistent with the errors of the sea level variance. Therefore, we

403   confirm that the discrepancies of sea level seasonality identified between the

404   two datasets are real and are not due to the methods used in the estimation.

405   **3.3 Temporal variability of the seasonal sea level cycle**

406   The temporal variability of the seasonal sea level cycle is produced by fitting

407   Eq.(3) into a 5-year segment of tide gauge records (η) with year-by-year shifting.

408   **Figure 5** shows the inter-annual variations of the seasonal sea level amplitudes

409   with respect to their own mean amplitudes for each station in the 6 sub-regions

410   (gray lines in the figure). The temporal changes for 5 outlier stations (station

411   number: 116-120) are provided in the supplementary material (**Figure S5**), and

412   at these stations the seasonal sea level cycle shows different temporal variability

413   in relation to the 6 sub-regions. Regional averages of the temporal changes in the

414   seasonal cycle are obtained by averaging all seasonal cycle amplitude anomalies

415   in one sub-region (black bold lines in **Figure 5**).

416   The annual and semi-annual sea level cycles are not constant in time (**Figure 5**).

417   The range between maximum and minimum A_a at individual stations usually

418   varies from 2cm to 8.6cm, with an average of 4.2cm (33% of their maximum

419   amplitudes). The largest ranges of 20.4cm and 16.5cm are observed at two

420   outliers in the south of Japan (station number: 116 and 117, see Figure S5). In

421   spite of apparent regional features, the inter-annual variability of A_a also shows

19

422   some consistency among regions. In particular, the significant change by ∼4 cm

423   for regional averages of A_a in the 1990's was present in all the regions. The

424   range of A_{sa} differences over time is 1-7 cm at individual stations, with an

425   average of 3.3cm (75% of their maximum amplitudes). The magnitudes of

426   temporal changes in the regional averages of A_{sa} are much smaller than those of

427   A_a. The consistency of the inter-annual variability of A_{sa} between different sub-

428   regions is only found in the North East of Japan and the Sea of Japan.

429

430   **4. Forcing of the seasonal sea level cycle**

431   **4.1 The IB effect and the steric height**

432   ***The IB effect (η_{IB})***

433   The mean seasonal sea level cycle of η_{IB} over 1993-2013 is mapped in **Figure 6**.

434   η_{IB} produces a significant annual sea level cycle over the whole area of study,

435   except in small areas in the Sea of Okhotsk and the central middle-latitude (30-

436   40°N) of Pacific. The annual cycle of η_{IB} exhibits the largest A_a (∼12cm) in the

437   middle of the continental shelf, i.e. the north of the East China Sea (**Figure 6a**).

438   η_{IB} has a uniform ϕ_a (July) over most areas, except in the north central Pacific

439   (35-60°N) where A_a is small and where ϕ_a varies by ∼6 months (**Figure 6b**).

440   The origin of the annual cycle of η_{IB} is linked with the strong seasonal variations

441   of the air pressure at high latitudes due to the radiational heating [*Yashayaev and*

442   *Zveryaev*, 2001; *Gabler et al.*, 2008].

443   The atmospherically-induced semi-annual sea level cycle is only distinguishable

444   at the mid-latitudes (30-50°N) of the north Pacific and the west of the South

445   China Sea (**Figure 6c**). The maximum A_{sa} of ~3cm are located at the center of

446   middle-to-high latitudes (around 43°N and 170°E), but the values are less than

447   1cm in most marginal seas. ϕ_{sa} is always in January or July, except in the Gulf of

448   Thailand (**Figure 6d**).

449   The inter-annual variability of the seasonal sea level cycle due to η_{IB} over the

450   same periods of tide gauge records was also calculated by using the long-term

451   atmospheric pressure data. Compared to η, η_{IB} for tide gauge records has very

452   limited inter-annual variability (less than 3cm) both in A_a and in A_{sa}. The ranges

453   between maximum and minimum A_a of η_{IB} at individual stations over time are

454   up to 2.4cm in the north of the East China Sea (station number: 48) and 2.7cm in

455   the Sea of Okhotsk (station number: 120). The weak impact of η_{IB} on the long-

456   term changes of the seasonal sea level cycle is also revealed in the regional

457   averages (see the supplementary material **Figure S6**).

458   ***The Steric height (η_{ster})***

459   The mean seasonal cycle of η_{ster} derived from EN4 over 1993-2013 is shown in

460   **Figure 7**. The annual cycle of η_{ster} is significant in the whole area of study, with

461   larger A_a at the mid-latitudes and along the Kuroshio Current. The strongest

462   signal with A_a of 12-14cm is found in the East China Sea, the east of the Sea of

463   Japan and the east of Japan. ϕ_a keeps homogeneous (~September) in the north

464   but it gradually shifts to January near the equator. The annual cycle in η_{ster} is

465   primarily determined by η_{thermo}. A_a of η_{halo} was found to be usually less than

466   1cm (not shown here). This is in agreement with the results by *Vinogradov et al.*

467   [2008].

468   The semi-annual cycle of η_{ster} is statistically significant in the tropics and the

469   north marginal seas (**Figure 7c**). The largest A_{sa} of 3cm is found in the east of

470   Philippines and around the north of Japan. ϕ_{sa} shifts quickly with different areas

471   (**Figure 7d**). The semi-annual cycle in η_{ster} is also mainly caused by η_{thermo}.

472   The inter-annual variability of the seasonal cycle in η_{ster} at locations at least

473   500m deep and closest to tide gauges was also estimated. The ranges of temporal

474   changes of A_a and A_{sa} in η_{ster} are close to those as observed in η. However, there

475   are only 32 (24) of the 120 stations where the inter-annual variability of A_a

476   (A_{sa}) between η_{ster} and η is significantly correlated (at 95% confidence level).

477   There is no change for the correlations when η_{IB} is removed from the observed η

478   (i.e. $\eta - \eta_{IB}$), confirming the conclusion drawn above that η_{IB} has very limited

479   influence on the long-term variability of the seasonal sea level cycle. The un-

480   robust relationship between η and η_{ster} for their seasonal cycles can also be

481   evidenced by the mismatching of their regional averages (see the supplementary

482   material **Figure S6**). Significant correlations for the regional averages only exist

483   for A_a over 1960-2013 in the east of the South China Sea, the East China Sea and

484   the southeast of Japan (R=0.69, 0.39 and 0.29 respectively).

485   When $\eta - \eta_{IB}$ and η_{ster} from SODA during 1900-2010 are being used, the inter-

486   annual variability of the seasonal amplitudes between the two sea level

487   components is significantly correlated in most areas, except in the Sea of

488   Okhotsk. η_{ster} explains more than 80% of inter-annual variations of A_a in $\eta - \eta_{IB}$

489   in the open ocean and the central South China Sea (**Figure 8**). At the coastal

490   regions, the relationships between η_{ster} and $\eta - \eta_{IB}$ at seasonal scales become

491   weak but still significant (at 95% confidence level), where η_{ster} explains 5-30%

492   of inter-annual variability of A_a in $\eta - \eta_{IB}$. The relationships at the coastal

493   regions are different from the un-robust correlations recognized between the

494   tide gauge records and EN4 data (above paragraph). This inconsistency can be

495   partly attributed to the fact that EN4 is an interpolated product which means

496   that the steric values at a single point over the slope are the result of integrating

497   observations from the shelf as well as from the open ocean. This is not the case in

498   an ocean model, in which every single point is representative of the variability on

499   its own location. On top of this, the length of tide gauge records may also have an

500   impact, as they are always shorter than the SODA re-analysis (111years).

501   Furthermore, it is also possible that SODA misses some processes that are

502   recorded by tide gauges. What we can confirm at this moment from the two

503   different assessments is that the contribution of η_{ster} to the inter-annual

504   variations of the seasonal sea level cycle along the coasts is not as robust as that

505   in the open ocean.

506   ***Residuals***

507   Removing η_{IB} and η_{ster} from the observed η permits the sea level residuals,

508    $\eta - \eta_{IB} - \eta_{ster}$, which have significantly reduced A_a in the East China Sea, the

509   Sea of Japan, the Luzon Strait and the open ocean, and at 89 of the 120 tide gauge

510   records (**Figure 9a**). We recall here that η_{ster} is appointed as the values at the

511   closest grid points over the continental slope (500 m deep). However, the annual

512   cycle of $\eta - \eta_{IB} - \eta_{ster}$ remains significant in most marginal seas and at 114 of

513   the 120 tide gauge records. A_a with values of 5-10cm are found in the East China

23

514   Sea, the Sea of Okhotsk and spots of the Kuroshio Extension region. It is worth

515   noting that the removal of η_{IB} and η_{ster} increases A_a by 5-10cm in the west of

516   the South China Sea. This confirms the finding by *Ponte* [2006] that η_{IB} has a

517   negative contribution to the monthly sea level variance in the Southeast Asia. ϕ_a

518   of $\eta - \eta_{IB} - \eta_{ster}$ varies gradually in each marginal sea, but more heterogeneous

519   features are found in the open ocean where A_a is low (**Figure 9b**).

520   The semi-annual cycle of $\eta - \eta_{IB} - \eta_{ster}$ is still significant at 98 tide gauge

521   stations and in most areas of marginal seas (**Figure 9c-d**). Removal of η_{IB} and

522   η_{ster} has limited influence on the semi-annual cycle in the marginal seas, except

523   in the Sea of Japan and the east of the Sea of Okhotsk. In these two areas, A_{sa}

524   increases by 2-4cm when the two effects are subtracted. The existence of the

525   seasonal cycle in $\eta - \eta_{IB} - \eta_{ster}$ indicates other mechanisms, beside η_{IB} and

526   η_{ster}, to force the seasonal sea level cycle (e.g. wind effects). Of course, we cannot

527   rule out the possibility that $\eta - \eta_{IB} - \eta_{ster}$ estimated here might be influenced

528   by the limitations of the dataset EN4 that is used to determine η_{ster}.

529   **4.2 Impacts from the wind stress and the sea surface currents**

530   As mentioned above, η_{IB} and η_{ster} cannot fully explain the whole budgets of the

531   observed seasonal sea level cycle either in its mean values or its inter-annual

532   variability, especially in the marginal seas. Therefore, in this subsection we

533   explored the potential contributions of the wind stress and the sea surface

534   currents by correlating the long-term seasonal cycle amplitudes. The wind stress

535   is expected to alter sea level variations via the mechanisms of ocean

536   upwelling/downwelling in coastal regions and water piling at the equator, which

24

537   are caused by the alongshore winds and the trade winds respectively through

538   the Ekman transport [*Segar*, 2007]. In the open ocean, the vertical Ekman

539   pumping due to the wind stress curl is able to produce the sea level variations as

540   well, especially for the steric component because of the thermocline changes.

541   The geostrophic balance is responsible for the mechanisms behind the links

542   between sea level and horizontal sea surface currents. We performed the

543   analyses in the seasonal cycle of $\eta - \eta_{IB}$ and $\eta - \eta_{IB} - \eta_{ster}$, to distinguish the

544   impacts of the two contributors on different components of sea level. The inter-

545   annual variability of A_a and A_{sa} for the wind stress and the sea surface currents

546   with different directions over 1900-2010 was calculated as mentioned in

547   subsection 2.5. Because AVISO records (21 years) are not long enough to fully

548   resolve the decadal changes in the seasonal sea level cycle and SODA, on the

549   other hand, is able to reasonably reproduce the seasonal sea level cycle (as

550   indicated in subsection 2.4), we used the sea surface height $\eta - \eta_{IB}$ from SODA

551   over the period 1900-2010 in this subsection instead, along with the observed

552      $\eta - \eta_{IB}$ from tide gauges over the same period.

553   ***Wind stress***

554   The best correlations of the inter-annual variability of A_a in $\eta - \eta_{IB}$ with that in

555   different directions of wind stress nearby (with 1° radius around the location of

556   sea level data) over 1900-2010 are shown in **Figure 10a**. The correlation

557   coefficient is significant (at 95% confidence level) at 90 of the 120 tide gauge

558   records and in most areas of the marginal seas. High correlations (R=0.6-0.9) are

559   found in the tropics and in the west areas of marginal seas. The direction of wind

560   stress that corresponds to the best correlations with sea level is provided in the

561   supplementary material (**Figure S7**). In the western areas of marginal seas the

562   annual cycle of sea level is better correlated with the zonal wind stress, while in

563   the north Japan and the open ocean it is better correlated with the meridional

564   wind stress component.

565   The regional averages of the inter-annual variability of A_a for tide gauge records

566   are well correlated with the corresponding quantity for the wind stress (**Figure**

567   **11a**), with R=0.58, 0.48, 0.59, 0.33, 0.48 and 0.41 over 1960-2010 for the 6 sub-

568   regions from south to north respectively. A_a of sea level is changing by about 2

569   cm for every 10^{-2} N/m² of changes in A_a of the wind stress for the regional

570   averages.

571   When η_{ster} is removed, the correlation of A_a between sea level and wind stress

572   remains nearly unchanged in the shallow waters of most marginal seas (**Figure**

573   **10b**), except in the west of the Sea of Japan. This means that the temporal

574   variations of the annual sea level cycle is dominated by $\eta - \eta_{IB} - \eta_{ster}$ and this

575   component is well related to the local wind. This identification could be

576   interpreted as the results of the coastal upwelling/downwelling or the wind-

577   driven sea surface currents in the coastal areas. **Figure 10** also shows that when

578   η_{ster} is excluded the relationship of sea level with wind stress disappears in the

579   central of the Sea of Japan, the central of the South China Sea and the tropics. The

580   annual cycle in η_{ster} over these areas can then be interpreted as wind stress-

581   dependent. This might be caused by the vertical Ekman pumping and the

582   equatorial upwelling that are both closely associated with the wind stress and

583   that are both significant for modulating the steric height.

584   The semi-annual sea level cycle has significant correlations with nearby wind

585   stress at 99 of the 120 tide gauge records and in large areas of marginal seas as

586   well (not shown here). The best agreements for A_{sa} between sea level

587   observations and the wind stress are in the northeast coasts of Japan and the

588   west coasts of the South China Sea (**Figure 11b**). Similarly as revealed in the

589   annual sea level cycle, the subtraction of η_{ster} does not apparently change the

590   correlations with the wind stress for A_{sa} in the marginal seas.

591   ***Sea surface currents***

592   The best correlations of the inter-annual variability of A_a between $\eta - \eta_{IB}$ and

593   the sea surface currents nearby are presented in **Figure 12a**. The correlation is

594   significant at 117 of the 120 tide gauge records and in most areas. The

595   relationships are stronger than those with the wind stress in most areas. Higher

596   correlations (R=0.7-0.95) appear in the regions where the ocean currents are

597   known to be strong, such as the Oyashio and Kuroshio Currents regions

598   [*Hurlburt et al.*, 1996] and the Luzon Strait [*Xue et al.*, 2004]. The direction of the

599   sea surface currents that is allocated to the best correlations with sea level varies

600   regionally except in subtropical areas where the associations seem to be more

601   determined by the meridional currents (**Figure S8** in supplementary). The fast

602   changes of the surface current direction for the best correlations indicate that

603   the geostrophic response of sea level might be acting locally and at small scales.

604   Also, we are aware that our method may not work well if the current direction

605   for the best correlations is changing in time. This limitation may cause fast

606   changes in the identified direction of the surface currents as well.

27

607 The regional averages of A_a anomalies of sea level from tide gauge observations

608 correlate well with the changes in the surface currents, with R=0.63, 0.45, 0.82,

609 0.71, 0.69 and 0.62 over 1960-2010 for the six sub-regions from south to north

610 respectively (**Figure 13a**). The regression for A_a is approximately 2 cm of

611 increase in sea level for 1 cm/s increase in the current speed. However, this scale

612 is greatly reduced prior to 1960 when the surface currents have larger range of

613 variations (**Figure 13a**). This is due to the fact that the magnitude of the

614 geostrophic response of sea level to nearby surface currents varies with

615 locations (see the supplementary material **Figure S9**) presumably because of

616 topography changes and thus the calculation of regional averages using fewer

617 individual records prior to 1960 (**Figure 1b**) leads to the average values that

618 reflect more localized features rather than the regional average features.

619 When η_{ster} is excluded from $\eta - \eta_{IB}$, A_a of sea level is still highly dependent on

620 the surface currents at 117 of the 120 tide gauge records, in the shallow waters

621 of marginal seas and in the north of the Oyashio Current region (**Figure 12b**).

622 This indicates that in these areas $\eta - \eta_{IB} - \eta_{ster}$ dominates the relationships of

623 $\eta - \eta_{IB}$ with the surface currents due to the geostrophic balance as expected.

624 This can be further evidenced by comparing the time series of A_a in η_{ster} and in

625 $\eta - \eta_{IB} - \eta_{ster}$ with the corresponding quantity in the surface currents at

626 specific points (**Figure 14a-b**). At location A [8°N, 108°E] in the Gulf of Thailand,

627 the inter-annual variability of A_a in η_{ster}, the dominating component in sea level,

628 is significantly correlated with the variability of the local surface current

629 (R=0.78). In contrast, changes in η_{ster} have no links with the current (R=0.1, not

630 significant at 95% confidence level). When location B [38°N, 123°E] in the East

28

631 China Sea is selected, A_a in η_{ster} becomes comparable to that in $\eta - \eta_{IB} - \eta_{ster}$.

632 The surface current has a significant correlation with η_{ster} (R=0.23), but it has an

633 even stronger correlation with $\eta - \eta_{IB} - \eta_{ster}$ (R=0.45).

634 However, the removal of η_{ster} eliminates the high correlations that are identified

635 for sea level in the open oceans, particularly in the areas of the south Oyashio,

636 the Kuroshio and the North Equatorial Currents, and in the Luzon Strait (**Figure**

637 **12**). The disappearance of correlations in these areas implies that η_{ster}, as the

638 dominating component of sea level in the open ocean, is firmly regulated by the

639 surface currents. Time series of the variables at two locations in these areas are

640 also plotted to support this argument (**Figure 14c-d)**. At location C [37°N,

641 143°E] on the route of the Kuroshio Current, the temporal variations of A_a

642 between η_{ster} and the surface current are very well matched (R=0.90). At

643 location D [4°N, 143°E] near to the North Equatorial Current, they are

644 significantly correlated as well but with a reduced correlation coefficient

645 (R=0.33).

646 It is worth noticing that the surface currents and the wind stress used in the

647 analysis cannot be independent. The inter-annual variability of their seasonal

648 cycles shows significant correlations in the marginal seas (except in the Sea of

649 Japan) and in the tropics, with R=0.7-0.95 (see the supplementary material

650 **Figure S10**). Thus, the relationships of sea level with the surface currents that

651 are found in the marginal seas and in the tropics (**Figure 12**) could be thought to

652 be the consequence of the impact from the local wind. However, no significant

653 correlations between the surface currents and the wind stress are found in the

654 open ocean, particularly in the regions with the strong currents, where no robust

655   correlations are found between sea level and the wind stress either (**Figure 10**).

656   Therefore, the high correlations of sea level with the surface currents in these

657   areas can be further interpreted as the consequence of the geostrophic balance

658   between η_{ster} and the large-scale ocean currents, which are not forced by the

659   local wind field.

660   The changes in A_{sa} of sea level are significantly correlated with the changes in

661   the surface currents at 117 tide gauge records and in most areas (not shown

662   here). The results for the regional averages of tide gauge records are shown in

663   **Figure 13b**. The correlations are again better than those obtained from the wind

664   stress.

665

666   **5. Conclusions**

667   The spatial and temporal features of the seasonal sea level variations in the

668   northwest Pacific have been described by investigating the sea level

669   observations from tide gauges (1900-2013) and gridded altimetry product

670   AVISO (1993-2013). In the marginal seas, 60-95% of the monthly sea level

671   variance can be explained by the annual and semi-annual cycles, except in the

672   Sea of Okhotsk where the seasonal sea level variance is weak and sea ice

673   becomes important [*Parkinson et al.,* 1999]. However, in the open ocean and

674   especially in eddy-rich regions (e.g. the Kuroshio Extension and the Oyashio

675   Current) where the monthly sea level is mainly driven by the mesoscale eddies,

676   the regular seasonal oscillations only account for 3-20% of the observed sea

677   level variance.

678   The annual sea level cycle is significant over the whole area of study, with A_a

679   over 10cm in the East China Sea, the Luzon Strait, the Gulf of Thailand and the

680   Kuroshio Current regions. The largest A_a of ~30 cm is observed in the north of

681   the East China Sea. The semi-annual sea level cycle is only significant along the

682   coasts and in the shallow waters of most marginal seas. The largest A_{sa} is ~6cm

683   on the northwestern coasts of the South China Sea. The seasonal cycle

684   parameters of sea level estimated from tide gauge records and AVISO were

685   compared. At the sites closest to tide gauge stations, AVISO significantly

686   underestimates A_a by 2-9cm (25%) at 59 of 120 stations and A_{sa} by 1-3 cm

687   (60%) at 28 stations. The discrepancies mainly occur on the coasts of China and

688   Russia.

689   The contributions of the IB effect (η_{IB}) and the steric height (η_{ster}) to the

690   observed seasonal sea level cycle have been identified. η_{IB} has significant impact

691   on the annual sea level cycle over the whole area of study, which causes the

692   largest A_a of 12cm in the East China Sea. The semi-annual cycle of η_{IB} is only

693   significant at the central north Pacific where A_{sa} is ~3cm. η_{ster}, mainly due to

694   the thermal expansion of seawater, can produce A_a with up to 8-12cm in the East

695   China Sea, the east of Sea of Japan and the Kuroshio Extension region. The

696   removal of η_{IB} and η_{ster} significantly diminishes the annual sea level cycle in

697   most areas, but increases the annual cycle by 5-10cm in the west of the South

698   China Sea. The removal has little impact on the semi-annual cycle. Significant

699   seasonal cycles still remain in the residuals over the marginal seas.

700   The long-term tide gauge observations allow us to assess the temporal

701   variability of the seasonal sea level variations on the coasts. The annual and

702 semi-annual sea level cycles are not stable with time, with amplitudes changing

703 between 2-20.4cm and 1-7cm respectively. η_{IB} and η_{ster} have limited influences

704 on the observed inter-annual variability of the seasonal sea level cycle based on

705 our analysis. However, in the open ocean η_{ster} explains over 80% of inter-annual

706 variations based on ocean reanalysis of SODA.

707 The dynamic forcing of the inter-annual variability in the seasonal sea level cycle

708 was also diagnosed using SODA data. The wind stress and especially the sea

709 surface currents are correlated with the seasonal sea level cycle at most tide

710 gauge records and in the marginal seas, as the consequence of their strong

711 contributions to the sea level residuals. The regional averages of the seasonal

712 cycle amplitudes are changing by ~2cm for 10^{-2} N/m^2 and 1 cm/s changes in the

713 amplitudes of the wind stress and the surface currents respectively. Because in

714 the marginal seas and in the tropics the seasonal variations of the currents are

715 highly dependent on the local wind stress, the relationships of sea level with the

716 surface currents observed here can be interpreted as the consequence of the

717 wind-driven Ekman transport. In the open ocean, especially in the regions of the

718 western boundary currents, the surface currents can better describe the

719 seasonal sea level variations (R=0.7-0.95) than the wind stress, and this is mainly

720 due to the significant associations between the steric height and the open ocean

721 currents through the geostrophic equilibrium. However, there are still some

722 areas in the open ocean, where neither the wind stress nor the surface currents

723 can well explain the forcing of the seasonal steric height variations which

724 account for over 80% of sea level changes. The vertical Ekman pumping caused

725   by the wind stress curl might be the reason and we will work on this in the

726   future.

727

747

Reference

Amiruddin, A. M., I. D. Haigh, M. N. Tsimplis, F. M. Calafat, and S. Dangendorf (2015), The seasonal cycle and variability of sea level in the South China Sea, *Journal of Geophysical Research: Oceans*, 120, doi:10.1002/2015JC010923

Anderson, C. J. and Lockaby, B. G. (2012), Seasonal patterns of river connectivity and saltwater intrusion in tidal freshwater forested wetlands, *River Research and Applications*, 28, 814–826, doi: 10.1002/rra.1489

Barbosa, S.M., M.E Silva, and M.J. Fernandes (2008), Changing seasonality in North Atlantic coastal sea level from the analysis of long tide gauge records, *Tellus A*, 60: 165–177, doi: 10.1111/j.1600-0870.2007.00280.x

Bingham, R. J., and C. W. Hughes (2012), Local diagnostics to estimate density-induced sea level variations over topography and along coastlines, *Journal of Geophysical Research: Oceans*, 117, C01013, doi:10.1029/2011JC007276.

Boyer, T. P., et al. (2009), World Ocean Database 2009, edited S. Levitus, 216 pp., NOAA Atlas NESDIS 66, U.S. Gov. Print. Off., Washington, D. C.

Carrère, L., and F. Lyard (2003), Modeling the barotropic response of the global ocean to atmospheric wind and pressure forcing - comparisons with observations, *Geophysical Research Letters*, 30(6), 1275, doi:10.1029/2002GL016473.

Carton, J. A., and B. S. Giese (2008), A reanalysis of ocean climate using Simple Ocean Data Assimilation (SODA), *Monthly Weather Review*, 136(8), 2999-3017, doi:10.1175/2007MWR1978.1.

Carton, J. A., G., Chepurin, X., Cao, and B., Giese (2000), A simple ocean data assimilation analysis of the global upper ocean 1950-95. Part I: Methodology, *Journal of Physical Oceanography*, 30(2), 294-309, doi:10.1175/1520-0485(2000)030<0294:ASODAA>2.0.CO;2.

Chelton, D. B., M. G. Schlax, and R. M. Samelson (2011), Global observations of nonlinear mesoscale eddies, *Progress in Oceanography*, 91, 167-216.

Chen, J. L., C. K. Shum, C. R. Wilson, D. P. Chambers, and B. D. Tapley (2000), Seasonal sea level change from TOPEX/Poseidon observation and thermal contribution, *Journal of Geodesy*, 73(12), 638-647, doi:10.1007/s001900050002.

Compo, G., et al. (2011), The twentieth century reanalysis project, *Quarterly Journal of the Royal Meteorological Society*, 137(654), 1–28, doi:10.1002/qj.776.

779   Dangendorf, S., C. Mudersbach, J. Jensen, G. Anette, and H. Heinrich (2013a), Seasonal to decadal
780   forcing of high water level percentiles in the German Bight throughout the last century, *Ocean*
781   *Dynamics*, 63(5), 533-548, doi: 10.1007/s10236-013-0614-4

782   Dangendorf, S., T. Wahl, C. Mudersbach, and J. Jensen (2013b), The Seasonal mean sea level cycle in
783   the Southeastern North Sea, *Journal of Coastal Research*, Special Issue No. 65, pp. 1915-1920,
784   ISSN 0749-0208

785   Feng, X., and M. N. Tsimplis (2014), Sea level extremes at the coasts of China, *Journal of Geophysical*
786   *Research: Oceans*, 119, 1593–1608, doi:10.1002/2013JC009607.

787   Feng, X., M. N. Tsimplis, and P. L. Woodworth (2015), Nodal variations and long-term changes in the
788   main tides on the coasts of China, *Journal of Geophysical Research: Oceans*, 120, 1215–1232,
789   doi:10.1002/2014JC010312.

790   Gabler, R., J., Petersen, L., Trapasso, and D., Sack (2008), Physical geography (ninth edition),
791   Cengage Learning, 672pp.

792   Giese, B. S. and S. Ray (2011), El Niño variability in simple ocean data assimilation (SODA), 1871–
793   2008, J. Geophys. Res., 116, C02024, doi:10.1029/2010JC006695.

794   Gill, A. E. (1982), Atmosphere-ocean dynamics (Vol. 30). Academic press.

795   Good, S. A., M. J. Martin, and N. A. Rayner (2013), EN4: Quality controlled ocean temperature and
796   salinity profiles and monthly objective analyses with uncertainty estimates, *Journal of*
797   *Geophysical Research: Oceans*, 118, 6704–6716, doi:10.1002/2013JC009067.

798   Haines, K., M. Valdivieso, H. Zuo, and V. N. Stepanov (2012), Transports and budgets in a 1/4 °
799   global ocean reanalysis 1989–2010, *Ocean Science*, 8, 333-344, doi:10.5194/os-8-333-2012

800   Hamlington, B.D., R.R, Leben, R.S. Nerem, and K.-Y. Kim (2010), New method for reconstructing sea
801   level from tide gauges using satellite altimetry, Geoscience and Remote Sensing Symposium
802   (IGARSS), 2010 IEEE International, pp.781-784, doi: 10.1109/IGARSS.2010.5651050

803   Hamlington, B. D., R. R. Leben, R. S. Nerem, W. Han, and K.-Y. Kim (2011), Reconstructing sea level
804   using cyclostationary empirical orthogonal functions, *Journal of Geophysical Research: Oceans,*
805   116, C12015, doi:10.1029/2011JC007529

806   Hamlington, B. D., R. R. Leben, L. A. Wright, and K.-Y. Kim (2012), Regional sea level
807   reconstruction in the Pacific ocean. *Marine Geodesy*, 35(sup1), 98-117, doi:
808   10.1080/01490419.2012.718210

809   Han, G., and W., Huang (2008), Pacific decadal oscillation and sea level variability in the Bohai,
810   Yellow, and East China seas, *Journal of Physical Oceanography*, 38(12), 2772-2783, doi:
811   10.1175/2008JPO3885.1.

812   Holgate, S. J., et al. (2012), New data systems and products at the permanent service for mean sea
813   level, *Journal of Coastal Research*, 29(3), 493-504, doi:10.2112/JCOASTRES-D-12-00175.1.

814 Hünicke, B., and E., Zorita (2008), Trends in the amplitude of Baltic Sea level annual cycle, *Tellus A*,
815   60: 154-164, doi: 10.1111/j.1600-0870.2007.00277.x

816 Hurlburt, H. E., A. J. Wallcraft, W. J. Schmitz Jr., P. J. Hogan, and E. J. Metzger (1996), Dynamics of
817   the Kuroshio/Oyashio current system using eddy-resolving models of the North Pacific Ocean,
818   *Journal of Geophysical Research: Oceans*, 101(C1), 941–976, doi:10.1029/95JC01674.

819 Kang, S. K., M. G. G. Foreman, H.-J. Lie, J.-H. Lee, J. Cherniawsky, and K.-D. Yum (2002), Two-
820   layer tidal modeling of the Yellow and East China Seas with application to seasonal variability of
821   the M_2 tide, *Journal of Geophysical Research: Oceans*, 107(C3), doi:10.1029/2001JC000838.

822 Marcos, M., and M. N. Tsimplis (2007), Variations of the seasonal sea level cycle in southern Europe,
823   *Journal of Geophysical Research: Oceans*, 112, C12011, doi:10.1029/2006JC004049.

824 Marcos, M., M. N. Tsimplis, and F. M. Calafat (2012), Inter-annual and decadal sea level variations in
825   the north-western Pacific marginal seas, *Progress in Oceanography*, 105, 4-21,
826   doi:10.1016/j.pocean.2012.04.010.

827 Müller, M., J. Cherniawsky, M. Foreman, and J.-S. von Storch (2014), Seasonal variation of the M2
828   tide, *Ocean Dynamics* 64(2), 159-177, doi:10.1007/s10236-013-0679-0.

829 Parkinson, C. L., D. J. Cavalieri, P. Gloersen, H. J. Zwally, and J. C. Comiso (1999), Arctic sea ice
830   extents, areas, and trends, 1978–1996, *Journal of Geophysical Research: Oceans,* 104(C9),
831   20837-20856, doi:10.1029/1999JC900082.

832 Pascual, A., M. Marcos, and D. Gomis (2008), Comparing the sea level response to pressure and wind
833   forcing of two barotropic models: Validation with tide gauge and altimetry data, *Journal of*
834   *Geophysical Research: Oceans*, 113, C07011, doi:10.1029/2007JC004459.

835 Passaro, M., P. Cipollini, and J. Benveniste (2015), Annual sea level variability of the coastal ocean:
836   The Baltic Sea-North Sea transition zone, *Journal of Geophysical Research: Oceans*, 120, 3061–
837   3078, doi:10.1002/2014JC010510.

838 Plag, H.-P., and M.N., Tsimplis (1999), Temporal variability of the seasonal sea-level cycle in the
839   North Sea and Baltic Sea in relation to climate variability, *Global and Planetary Change*, 20,
840   173-203, doi:10.1016/S0921-8181(98)00069-1

841 Ponte, R. M. (2006), Low-frequency sea level variability and the inverted barometer effect, *Journal of*
842   *Atmospheric and Oceanic Technology*, 23(4), 619-629, doi: 10.1175/JTECH1864.1.

843 Pugh, D. and P. Woodworth (2014), Sea-level science: understanding tides, surges, tsunamis and mean
844   sea-level changes , Cambridge University Press , UK 395 pp.

845 Segar, D.A. (2007), Introduction to Ocean Sciences, W. W. Norton and Company, Inc., New York,
846   U.S.A. 720pp.

847 Smith, R. D., J. K., Dukowicz, and R. C., Malone (1992), Parallel ocean general circulation modeling,
848   *Physica D: Nonlinear Phenomena*, 60(1), 38-61, doi: 10.1016/0167-2789(92)90225-C.

849   Tabata, S., B., Thomas, and D., Ramsden (1986), Annual and interannual variability of steric sea level
850   along line P in the northeast Pacific Ocean, *Journal of Physical Oceanography*, 16(8), 1378-
851   1398. doi: 10.1175/1520-0485(1986)016<1378:AAIVOS>2.0.CO;2.

852   Tamisiea, M. E., E. M. Hill, R. M. Ponte, J. L. Davis, I. Velicogna, and N. T. Vinogradova (2010),
853   Impact of self-attraction and loading on the annual cycle in sea level, *Journal of Geophysical*
854   *Research-Oceans*, 115, C07004, doi:10.1029/2009JC005687

855   Torres, R. R., and M. N. Tsimplis (2012), Seasonal sea level cycle in the Caribbean Sea, *Journal of*
856   *Geophysical Research: Oceans*, 117, C07011, doi:10.1029/2012JC008159.

857   Tsimplis, M. N., and P. L. Woodworth (1994), The global distribution of the seasonal sea level cycle
858   calculated from coastal tide gauge data, *Journal of Geophysical Research*, 99(C8), 16031–16039,
859   doi:10.1029/94JC01115.

860   Tsimplis, M. N. and A. G. P. Shaw (2010), Seasonal sea level extremes in the Mediterranean Sea and
861   at the Atlantic European coasts, *Natural Hazards and Earth System Sciences*, 10, 1457-1475,
862   doi:10.5194/nhess-10-1457-2010

863   UNESCO (1981), Tenth Report of the International oceanographic Tables. UNESCO Technical Papers
864   in Marine Science 36, 25.

865   Vignudelli S., Kostianoy A. G., Cipollini P., Benveniste J. (Editors) (2011), Coastal Altimetry,
866   Springer-Verlag Berlin Heidelberg, 578 pp, doi:10.1007/978-3-642-12796-0.

867   Vinogradov, S. V., and R. M. Ponte (2010), Annual cycle in coastal sea level from tide gauges and
868   altimetry, *Journal of Geophysical Research: Oceans*, 115, C04021, doi:10.1029/2009JC005767.

869   Vinogradov, S. V., R. M. Ponte, P. Heimbach, and C. Wunsch (2008), The mean seasonal cycle in sea
870   level estimated from a data-constrained general circulation model, *Journal of Geophysical*
871   *Research: Oceans*, 113, C03032, doi:10.1029/2007JC004496.

872   Wahl, T., F. M. Calafat, and M. E. Luther (2014), Rapid changes in the seasonal sea level cycle along
873   the US Gulf coast from the late 20th century, *Geophysical Research Letters*, 41, 491–498,
874   doi:10.1002/2013GL058777.

875   Woodruff, S. D., et al. (2011), ICOADS Release 2.5: extensions and enhancements to the surface
876   marine meteorological archive, *International Journal of Climatology*, 31: 951–967. doi:
877   10.1002/joc.2103.

878   Wunsch, C., and D. Stammer (1997), Atmospheric loading and the oceanic "inverted barometer"
879   effect, *Reviews of Geophysics*, 35(1), 79–107, doi:10.1029/96RG03037.

880   Xue, H., F. Chai, N. Pettigrew, D. Xu, M. Shi, and J. Xu (2004), Kuroshio intrusion and the circulation
881   in the South China Sea, *Journal of Geophysical Research*, 109, C02017,
882   doi:10.1029/2002JC001724.

883   Yashayaev, I. M. and Zveryaev, I. I. (2001), Climate of the seasonal cycle in the North Pacific and the
884   North Atlantic oceans. *International Journal of Climatology*, 21: 401–417. doi:10.1002/joc.585.

885   Wang, W., H. Liu, Y. Li, and J. Su (2014), Development and management of land reclamation in

886   China, *Ocean and Coastal Management*, 102, 415-425. doi:10.1016/j.ocecoaman.2014.03.009.

887

888

889 **Figure 1.**
890 Study areas and locations of 120 tide gauges (**a**), and periods of valid η observed
891 from tide gauges (**b**). Tide gauges are colored and numbered into six sub-regions,
892 with five stations treated as outliers (black dots). The six sub-regions are named
893 as the east of the South China Sea (SCS-E), the west of the South China Sea (SCS-
894 W), the East China Sea (ECS), the Sea of Japan (SoJ), the northeast coasts of Japan
895 (Japan-NE) and the southeast coasts of Japan (Japan-SE). KS, LS and GTL
896 represent the Korea Strait, the Luzon Strait and the Gulf of Thailand respectively.
897
898 **Figure 2.**
899 Variance of η observed from tide gauges and AVISO (**a**), and percentage of the
900 variance explained by the seasonal cycle (**b**). Schematic routes of the Oyashio,
901 the Kuroshio and the North Equatorial Currents are indicated by the black
902 dashed lines in (**a**), which are estimated using the altimeter data distributed by
903 AVISO.
904
905 **Figure 3.**
906 Mean A_a (**a**), ϕ_a (**b**), A_{sa} (**c**) and ϕ_{sa} (**d**) of η from tide gauges and AVISO. Blank
907 areas and circles indicate the estimates of the annual or semi-annual cycle
908 parameters that are not passing the significance test at 95% confidence level.
909
910 **Figure 4.**
911 Differences of mean A_a (**a**), ϕ_a (**b**), A_{sa} (**c**) and ϕ_{sa} (**d**) of η determined by tide
912 gauges and AVISO at the closest points to tide gauges (TG) (AVISO – tide gauges).
913 Black bars indicate the differences that pass the significance test, i.e. error bars
914 of two estimated values (one from AVISO and the other from tide gauges) used in
915 comparison do not overlap, while grey bars indicate the insignificant differences.
916
917 **Figure 5.**
918 Time series of the anomaly of A_a (**a**) and A_{sa} (**b**) of η determined from tide
919 gauges, which are grouped by 6 sub-regions as specified in **Figure 1**. Bold black
920 line is plotted for the regional ensemble average of individual anomalies in each
921 sub-region.
922
923 **Figure 6.**
924 Mean A_a (**a**), ϕ_a (**b**), A_{sa} (**c**) and ϕ_{sa} (**d**) for η_{IB} derived from DAC data over
925 1993-2013. Blank areas indicate the estimates of the annual or semi-annual cycle
926 parameters that are not passing the significance test at 95% confidence level.
927 Pleasse note that the scales of amplitudes here are different from those in **Figure**
928 **3**.
929
930 **Figure 7.**
931 Mean A_a (**a**), ϕ_a (**b**), A_{sa} (**c**) and ϕ_{sa} (**d**) for η_{ster} derived from EN4 over 1993-
932 2013. Blank areas indicate the estimates of the annual or semi-annual cycle
933 parameters that are not passing the significance test at 95% confidence level.
934 Pleasse note that the scales of amplitudes here are different from those in **Figure**
935 **3**.
936
937

938 **Figure 8.**
939 Percentage of the inter-annual variability of A_a (**a**) and A_{sa} (**b**) for $\eta - \eta_{IB}$
940 explained by that of η_{ster} over 1900-2010, derived from SODA. Blank areas
941 indicate the girds where the correlation of the inter-annual variability of A_a or
942 A_{sa} between $\eta - \eta_{IB}$ and η_{ster} are not significant at 95% confidence level.
943
944 **Figure 9.**
945 Mean A_a (**a**), ϕ_a (**b**), A_{sa} (**c**) and ϕ_{sa} (**d**) for $\eta - \eta_{IB} - \eta_{ster}$ when η_{IB} and η_{ster}
946 are removed from η provided by tide gauges and AVISO. Blank circles and areas
947 indicate the estimates of the annual or semi-annual cycle parameters that are not
948 passing the significance test at 95% confidence level.
949
950 **Figure 10**.
951 (**a**) Best correlation coefficients of the inter-annual variability of A_a between
952 $\eta - \eta_{IB}$, provided by tide gauges and SODA, and the nearby wind stress; (**b**) same
953 as (**a**), but for the correlations between $\eta - \eta_{IB} - \eta_{ster}$ and the nearby wind
954 stress. Blank circles and areas indicate the correlations that do not pass the
955 significance test at 95% confidence level. Note that the direction of wind stress
956 corresponding to the best correlation coefficients is provided in the
957 supplementary material **Figure S7**.
958
959 **Figure 11**.
960 Time series of regional average anomaly of A_a (**a**) and A_{sa} (**b**) for $\eta - \eta_{IB}$ (black)
961 against the corresponding average of the wind stress (red) in 6 sub-regions as
962 specified in **Figure 1**.
963
964 **Figure 12.**
965 Same as **Error! Reference source not found.**, but for best correlations with the
966 nearby sea surface currents. Black dots in (**a**) highlight 4 grid points: A [8°N,
967 108°E], B [38°N, 123°E], C [37°N, 143°E] and D[4°N, 143°E]. Note that the
968 direction of surface currents corresponding to the best correlation coefficients
969 with sea level is provided in the supplementary material **Figure S8**.
970
971 **Figure 13**.
972 Same as **Figure 11**, but for time series of the sea surface currents (red).
973
974 **Figure 14.**
975 Time series of A_a for $\eta - \eta_{IB} - \eta_{ster}$ (green) and η_{ster} (red), along with the
976 corresponding quantity of the sea surface currents that are best corrected with
977 time series for $\eta - \eta_{IB}$, at 4 grid points A-D (**a-d**) as indicated in Error! Reference
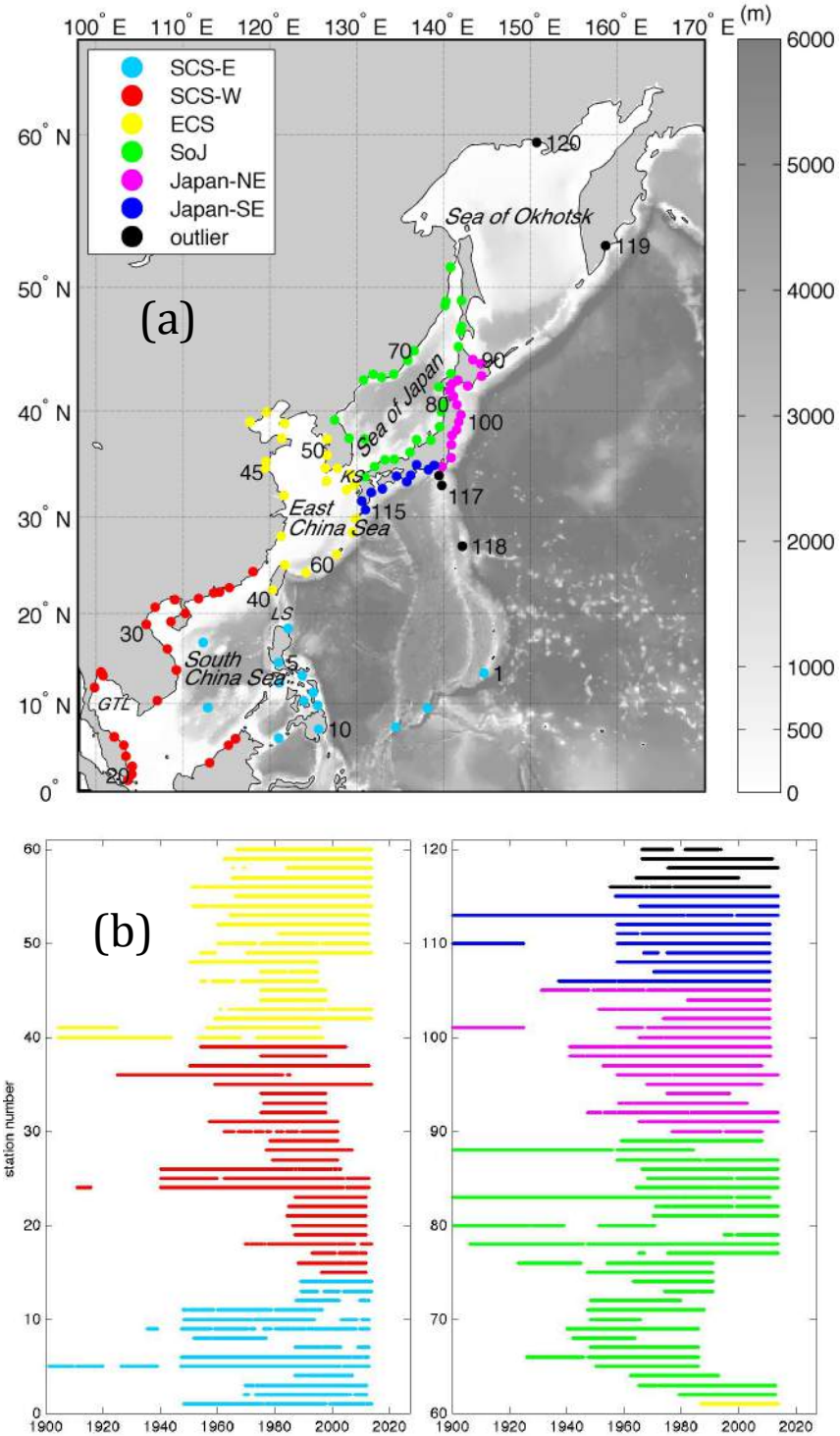978 source not found.**a**.

Figure 1. Study areas and locations of 120 tide gauges (**a**), and periods of valid η observed from tide gauges (**b**). Tide gauges are colored and numbered into six sub-regions, with five stations treated as outliers (black dots). The six sub-regions are named as the east of the South China Sea (SCS-E), the west of the South China Sea (SCS-W), the East China Sea (ECS), the Sea of Japan (SoJ), the northeast coasts of Japan (Japan-NE) and the southeast coasts of Japan (Japan-SE). KS, LS and GTL represent the Korea Strait, the Luzon Strait and the Gulf of Thailand respectively.
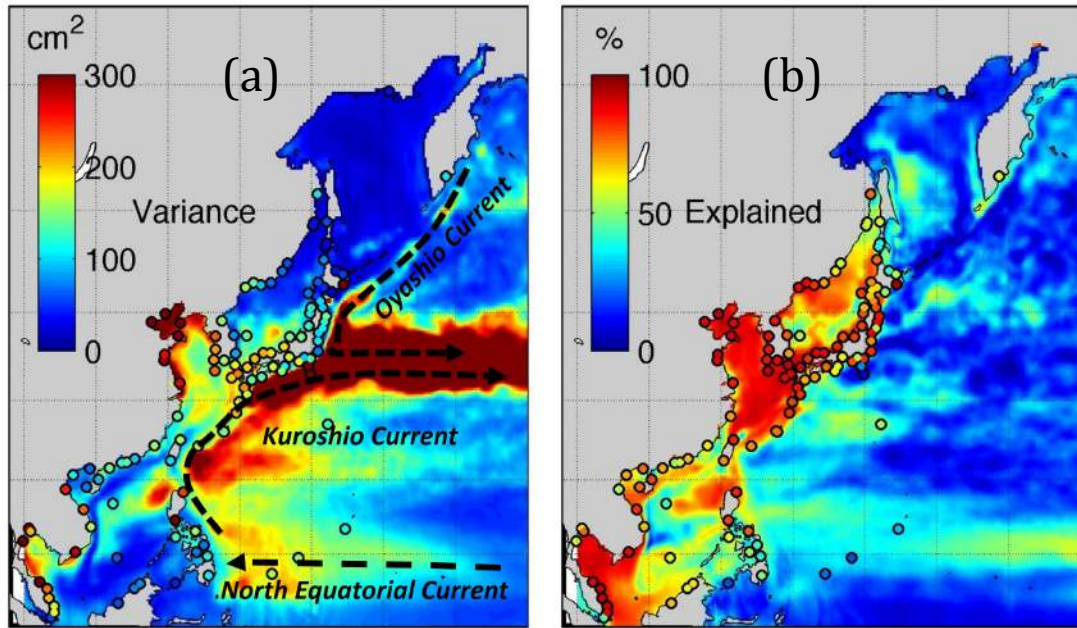
Figure 2. Variance of η observed from tide gauges and AVISO (**a**), and percentage of the variance explained by the seasonal cycle (**b**). Schematic routes of the Oyashio, the Kuroshio and the North Equatorial Currents are indicated by the black dashed lines in (**a**), which are estimated using the altimeter data distributed by AVISO.
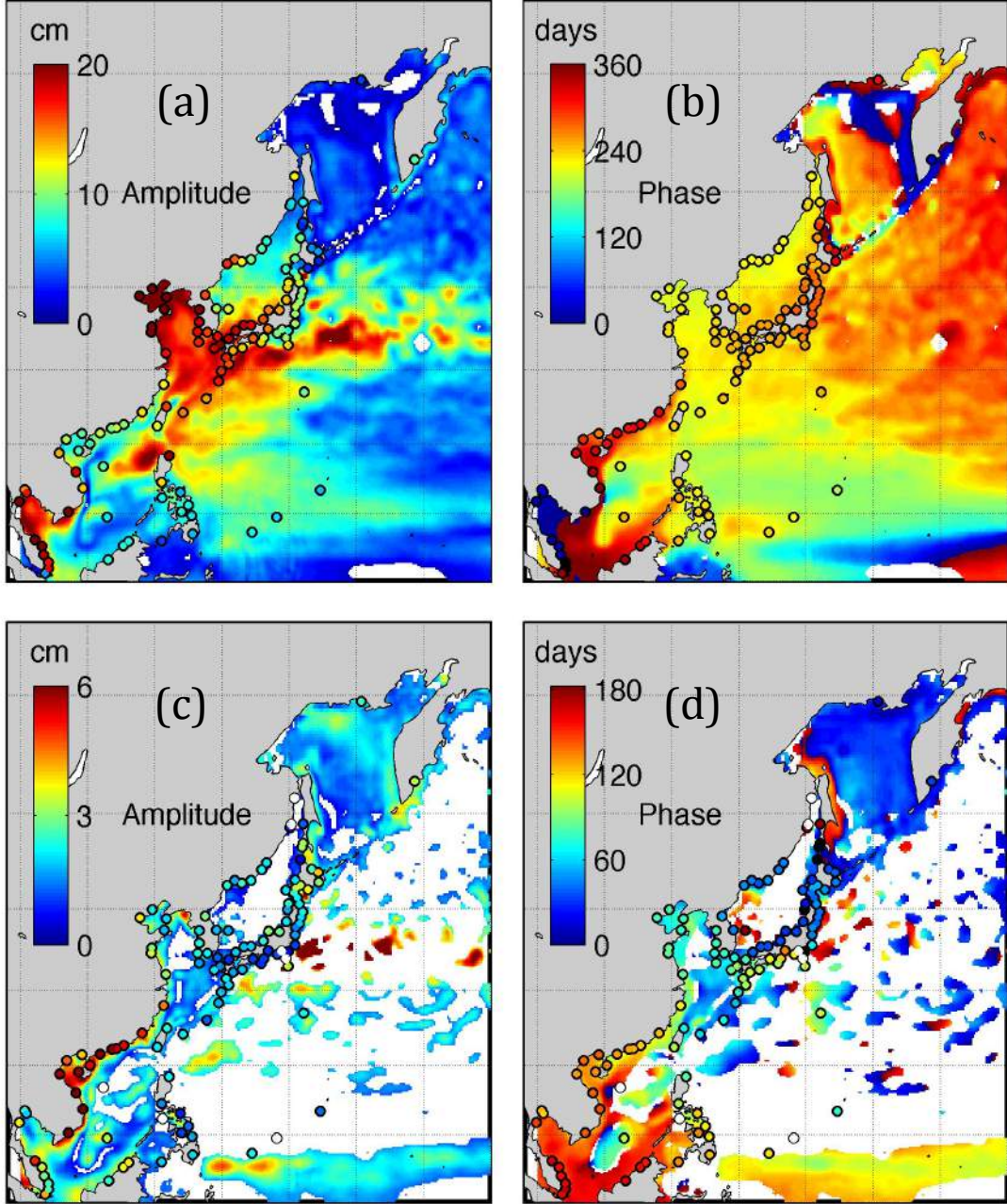
Figure 3. Mean A_a (**a**), ϕ_a (**b**), A_{sa} (**c**) and ϕ_{sa} (**d**) of η from tide gauges and AVISO. Blank areas and circles indicate the estimates of the annual or semi-annual cycle parameters that are not passing the significance test at 95% confidence level.
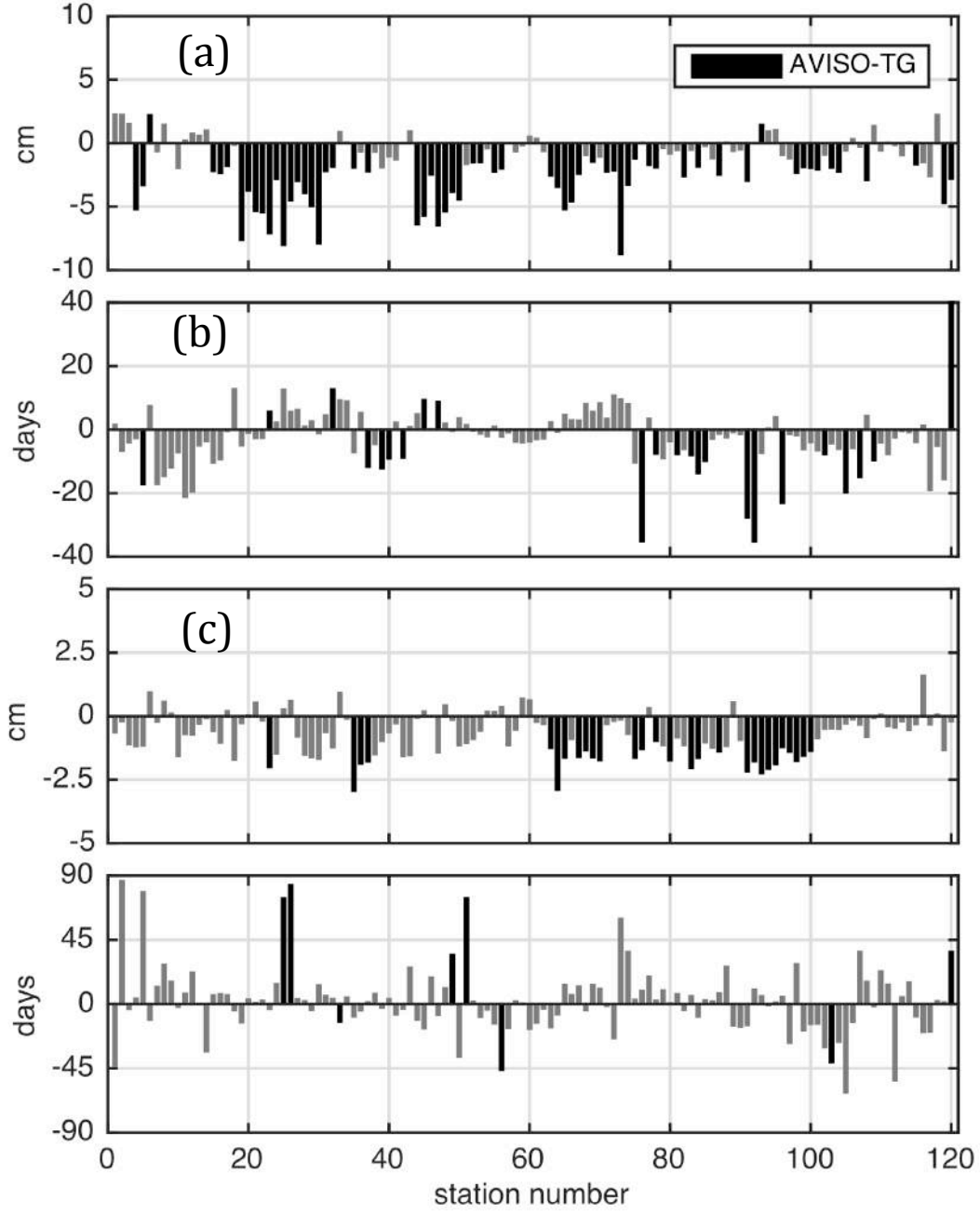
Figure 4. Differences of mean A_a (**a**), ϕ_a (**b**), A_{sa} (**c**) and ϕ_{sa} (**d**) of η determined by tide gauges and AVISO at the closest points to tide gauges (TG) (AVISO – tide gauges). Black bars indicate the differences that pass the significance test, i.e. error bars of two estimated values (one from AVISO and the other from tide gauges) used in comparison do not overlap, while grey bars indicate the insignificant differences.

4
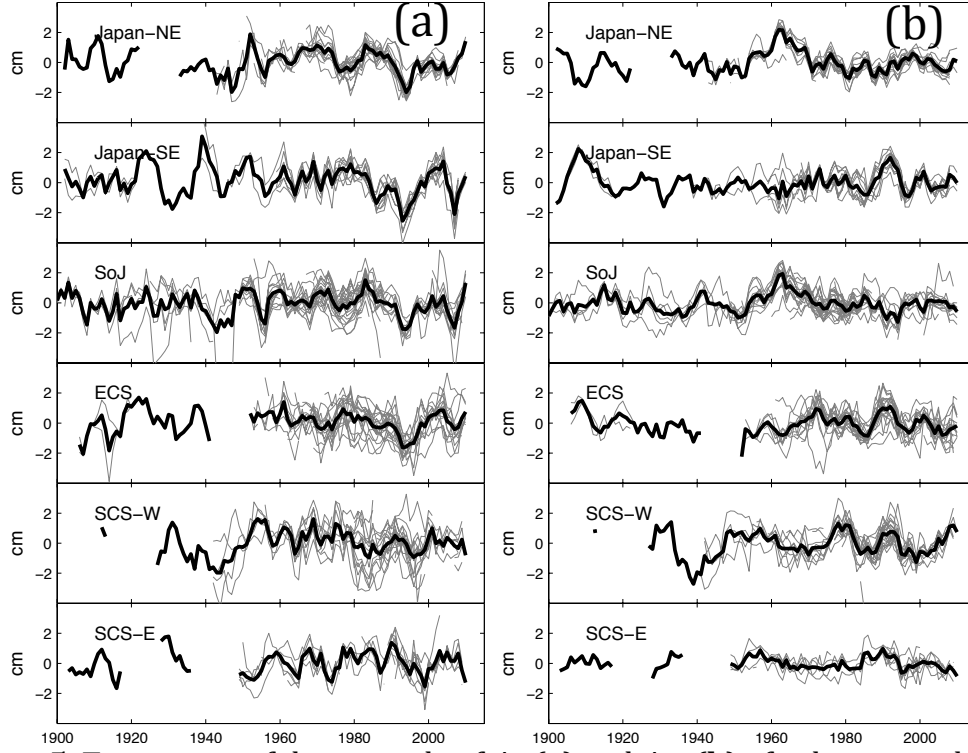
Figure 5. Time series of the anomaly of A_a (**a**) and A_{sa} (**b**) of η determined from tide gauges, which are grouped by 6 sub-regions as specified in **Figure 1**. Bold black line is plotted for the regional ensemble average of individual anomalies in each sub-region.
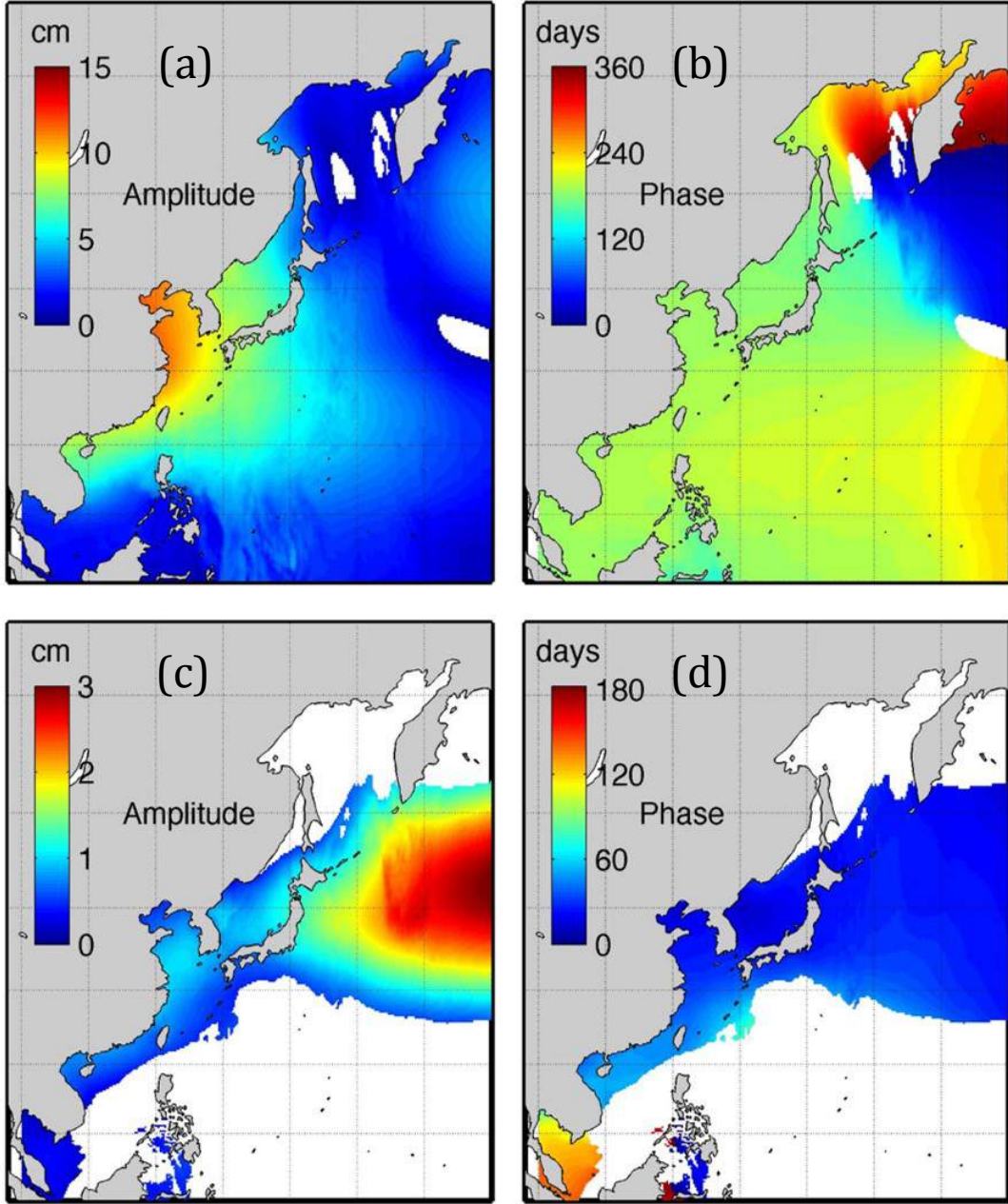
Figure 6. Mean A_a (**a**), ϕ_a (**b**), A_{sa} (**c**) and ϕ_{sa} (**d**) for η_{IB} derived from DAC data over 1993-2013. Blank areas indicate the estimates of the annual or semi-annual cycle parameters that are not passing the significance test at 95% confidence level. Pleasse note that the scales of amplitudes here are different from those in **Figure 3**.
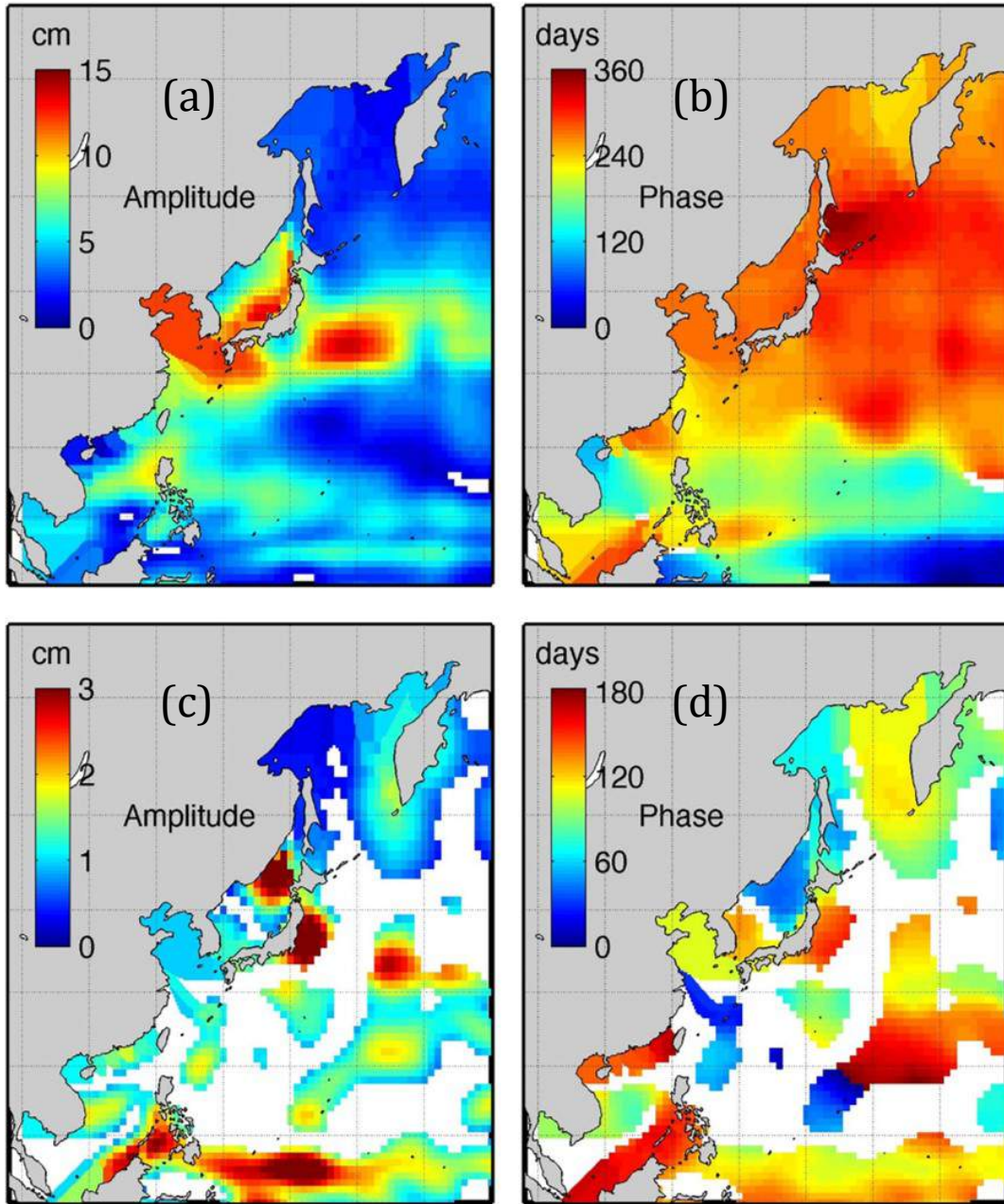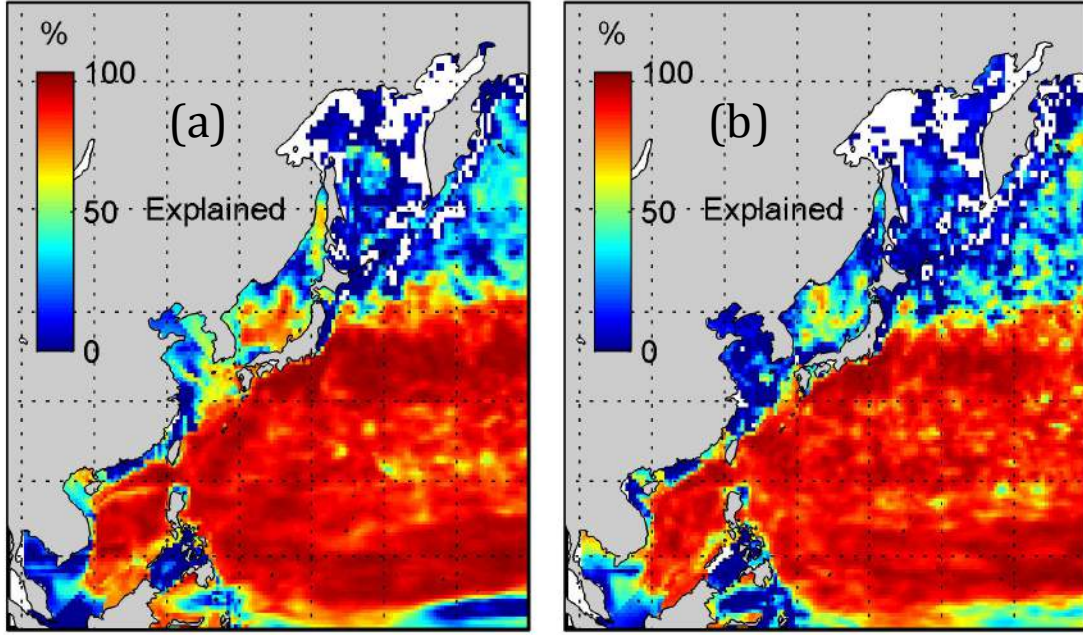
Figure 7. Mean A_a (**a**), ϕ_a (**b**), A_{sa} (**c**) and ϕ_{sa} (**d**) for η_{ster} derived from EN4 over 1993-2013. Blank areas indicate the estimates of the annual or semi-annual cycle parameters that are not passing the significance test at 95% confidence level. Pleasse note that the scales of amplitudes here are different from those in **Figure 3**.

Figure 8. Percentage of the inter-annual variability of A_a (**a**) and A_{sa} (**b**) for $\eta - \eta_{IB}$ explained by that of η_{ster} over 1900-2010, derived from SODA. Blank areas indicate the girds where the correlation of the inter-annual variability of A_a or A_{sa} between $\eta - \eta_{IB}$ and η_{ster} are not significant at 95% confidence level.
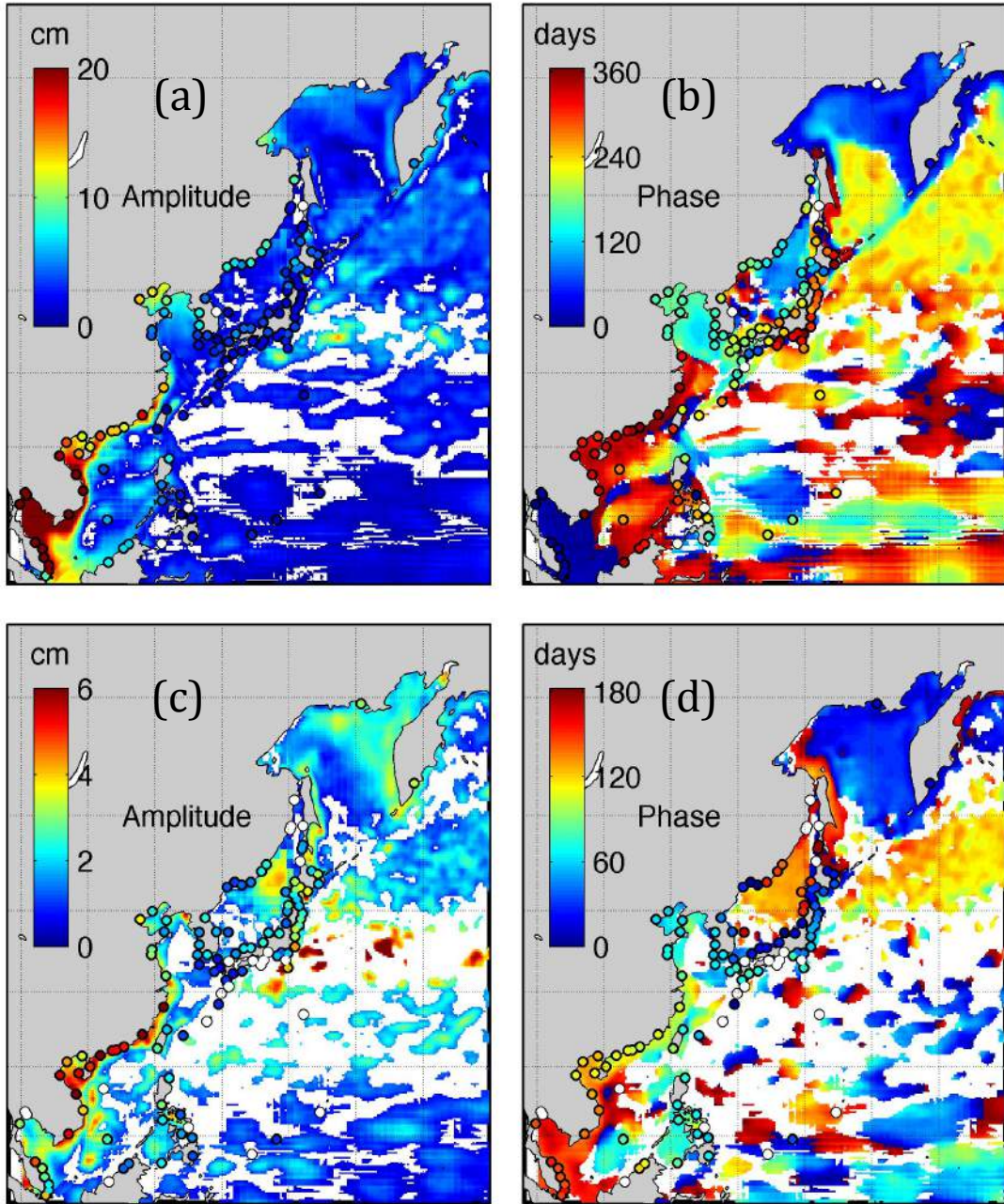
Figure 9. Mean A_a (**a**), ϕ_a (**b**), A_{sa} (**c**) and ϕ_{sa} (**d**) for $\eta - \eta_{IB} - \eta_{ster}$ when η_{IB} and η_{ster} are removed from η provided by tide gauges and AVISO. Blank circles and areas indicate the estimates of the annual or semi-annual cycle parameters that are not passing the significance test at 95% confidence level.
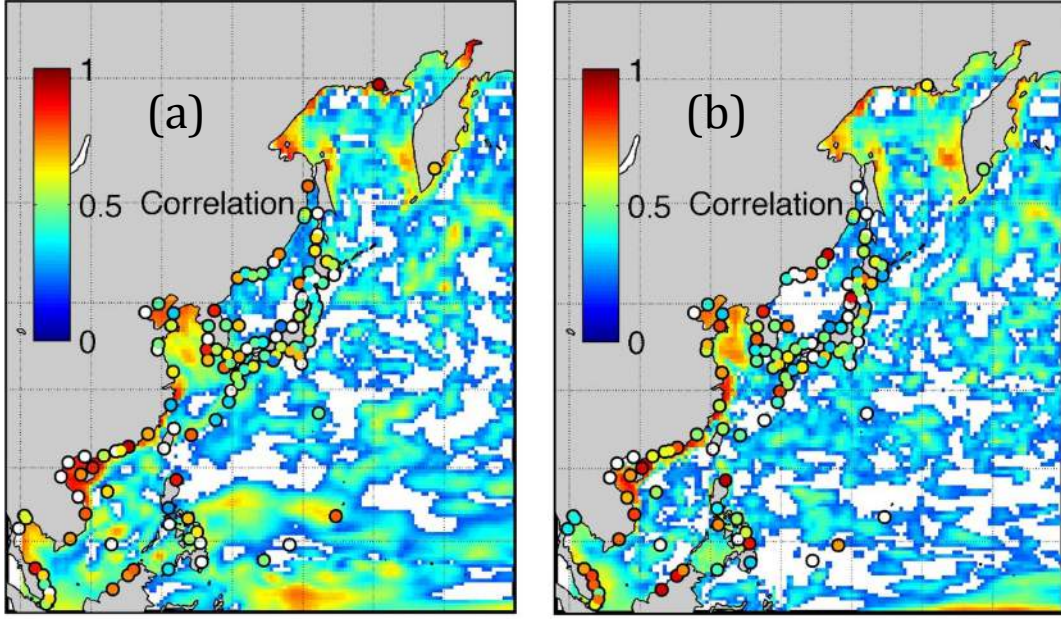
Figure 10. (**a**) Best correlation coefficients of the inter-annual variability of A_a between $\eta - \eta_{IB}$, provided by tide gauges and SODA, and the nearby wind stress; (**b**) same as (**a**), but for the correlations between $\eta - \eta_{IB} - \eta_{ster}$ and the nearby wind stress. Blank circles and areas indicate the correlations that do not pass the significance test at 95% confidence level. Note that the direction of wind stress corresponding to the best correlation coefficients is provided in the supplementary material **Figure S7**.
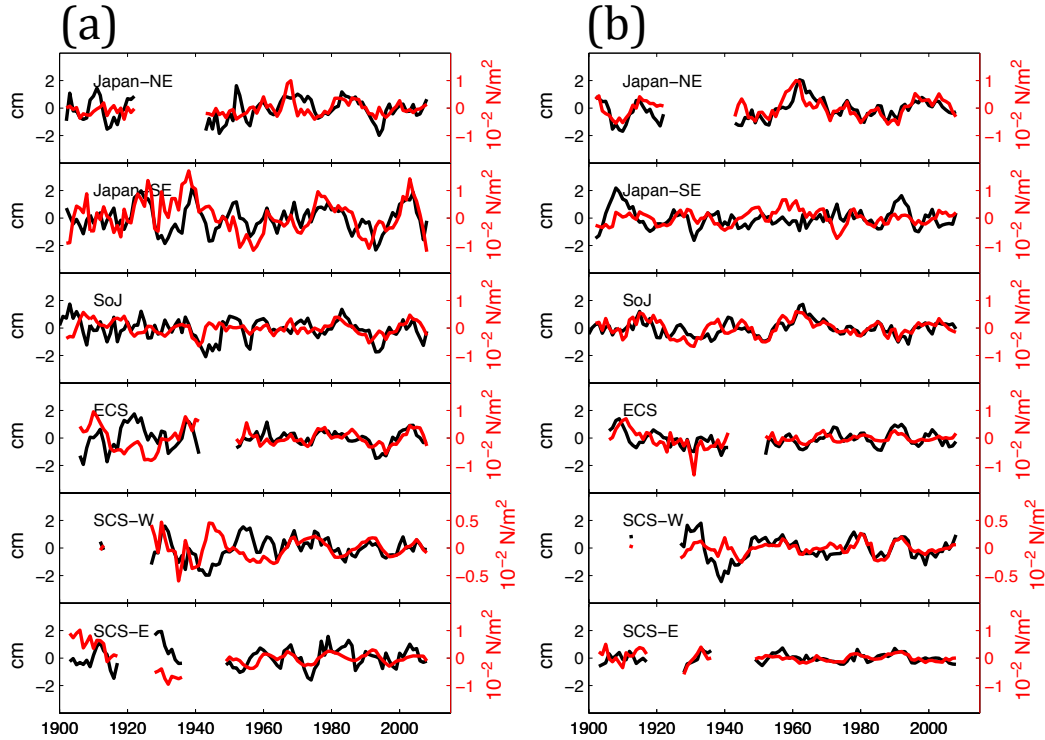
Figure 11. Time series of regional average anomaly of A_a (**a**) and A_{sa} (**b**) for $\eta - \eta_{IB}$ (black) against the corresponding average of the wind stress (red) in 6 sub-regions as specified in **Figure 1**.
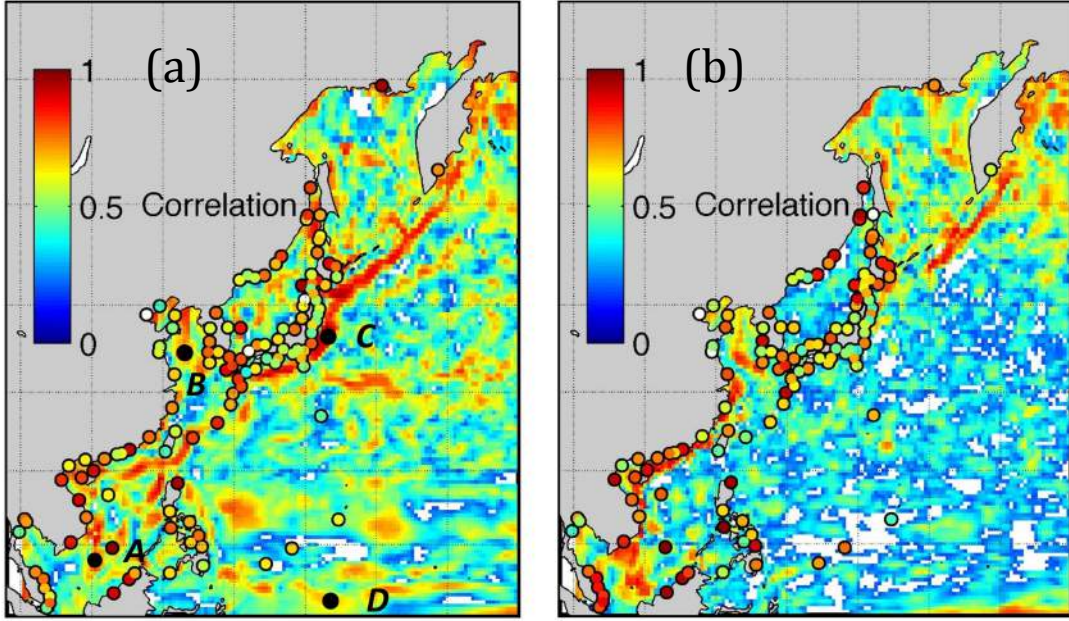
10

Figure 12. Same as **Figure 10**, but for best correlations with the nearby sea surface currents. Black dots in (**a**) highlight 4 grid points: A [8°N, 108°E], B [38°N, 123°E], C [37°N, 143°E] and D[4°N, 143°E]. Note that the direction of surface currents corresponding to the best correlation coefficients with sea level is provided in the supplementary material **Figure S8**.
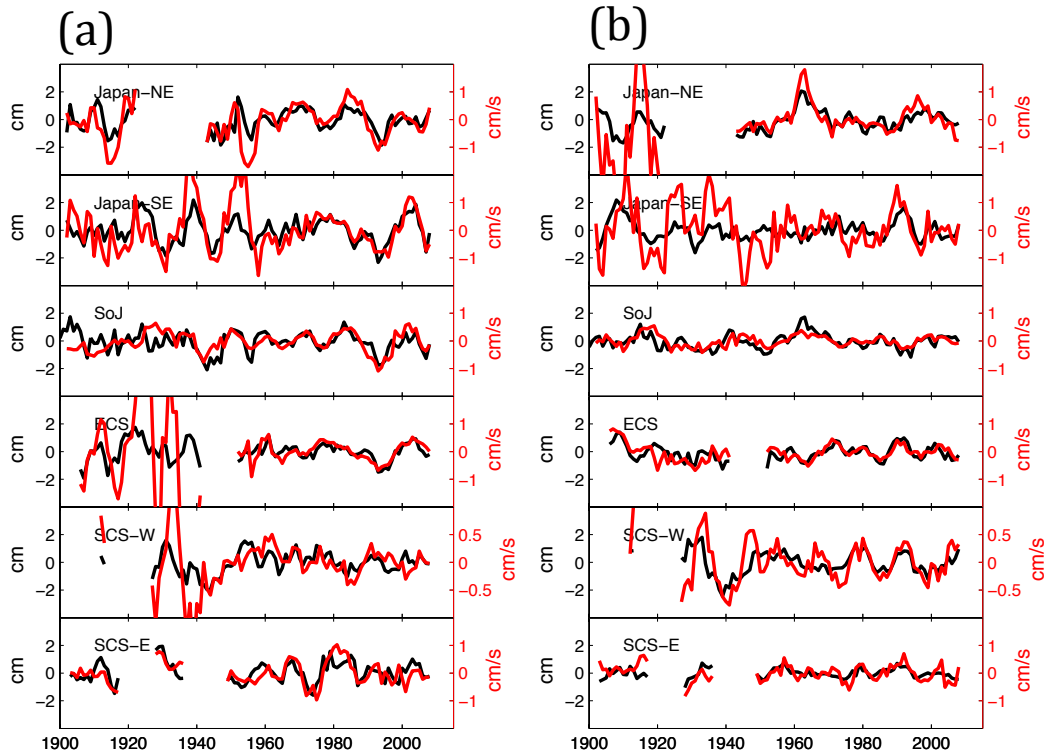

Figure 13. Same as **Figure 11**, but for time series of the sea surface currents (red).
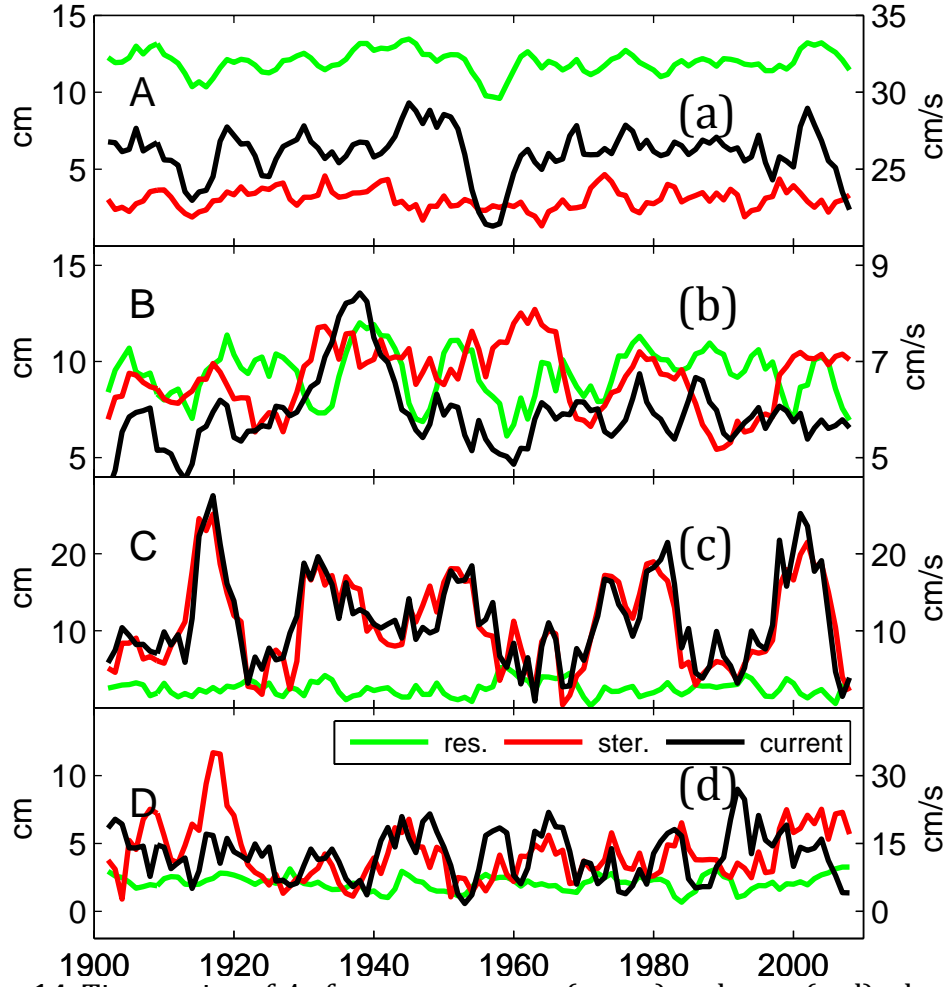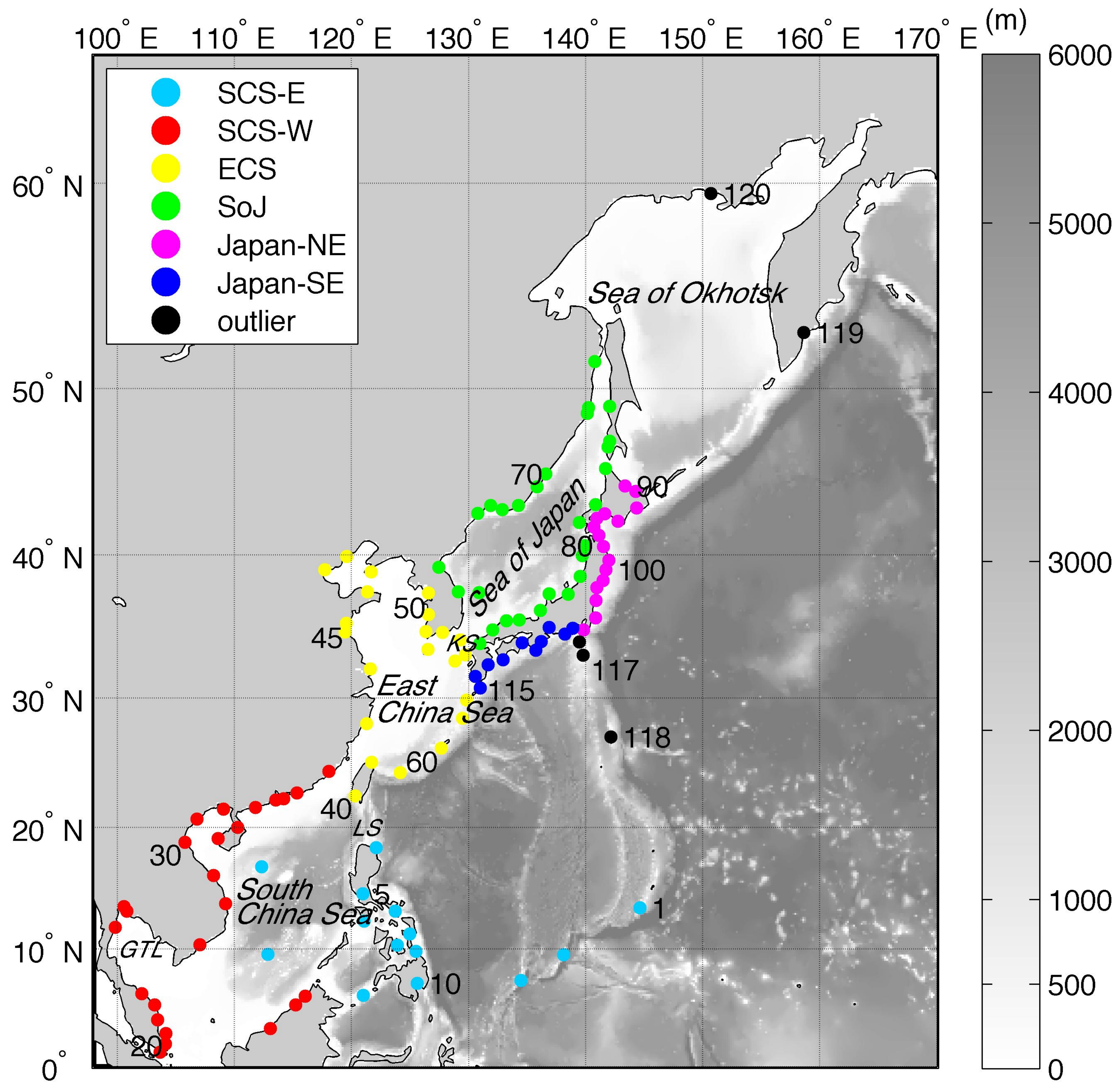
11

Figure 14. Time series of A_a for $\eta - \eta_{IB} - \eta_{ster}$ (green) and η_{ster} (red), along with the corresponding quantity of the sea surface currents that are best corrected with time series for $\eta - \eta_{IB}$, at 4 grid points A-D (**a-d**) as indicated in **Figure 12a**.

Left panel: cm² scale (0–300) labeled "Variance", with currents labeled Oyashio Current, Kuroshio Current, and North Equatorial Current. Right panel: % scale (0–100) labeled "Explained".